Supporting Information for

Acid-base interactions in luminescent silver(I) and gold(I) complexes with phosphine-phosphinate/phosphinite ligands

Mariia Beliaeva,[a] Andrey Belyaev,[a] Henna Korhonen,[a] Ondrej Mrózek,[b] Janne Jänis,[a] Andreas Steffen,[b] Igor O. Koshevoy[a]**

[a] *Department of Chemistry and Sustainable Technology, University of Eastern Finland, Yliopistokatu 7, Joensuu, 80101, Finland*

[b] *Department of Chemistry and Chemical Biology, TU Dortmund University, Otto-Hahn-Str. 6, 44227 Dortmund, Germany*

E-mail: andreas.steffen@tu-dortmund.de; igor.koshevoy@uef.fi

Table of Contents

Experimental

General comments. (2-Bromophenyl)diphenylphosphine,[1] chloro(tetrahydrothiophene)gold(I) (Au(tht)Cl),[2] silver phenylacetylide (AgC_2Ph),[3] bis(2-(diphenylphosphaneyl)phenyl)phosphine oxide (H***P*³*O***),[4] [Ag_2(***P*³*O***)$_2$][4] [Au_2(***P*³*O***)$_2$][5] were prepared according to the published procedures. Organic solvents for the syntheses and photophysical measurements were of HPLC grade. Tetrahydrofuran (THF) and toluene for the preparation of the phosphine ligand were distilled over Na-benzophenone ketyl under a nitrogen atmosphere prior to use. Dichloromethane and THF for the preparation of complexes were purified in a PureSolv MD 7 solvent purification system and further degassed by freeze-pump-thaw technique. Other reagents and solvents were used as received. All reactions were carried out under an inert nitrogen or argon atmosphere. The solution ^{1}H, ^{31}P{^{1}H}, ^{19}F{^{1}H}, ^{31}P–^{31}P COSY NMR spectra were recorded on Bruker 400 MHz Avance, Avance III HD NanoBay-400 MHz, Avance NEO-500 MHz, AMX-400 MHz and JEOL-500 MHz spectrometers. Mass spectrometry experiments were performed on an Agilent 6560 ESI-IM-QTOF and Agilent 6530 UHPLC-QTOF mass spectrometers equipped with AJS ESI ion source. Samples were injected using direct infusion from a syringe pump with a flowrate of 5 µl/min. Nitrogen was used as dry-, sheath and nebulizer gas from nitrogen generator. A dry-gas temperature of 225º C, drying gas flow rate of 5 l/min, nebulizer pressure of 30 psi, sheath gas temperature of 225º C and sheath gas flow of 10 l/min were used. Capillary voltage of 2000 V and fragmentation voltage of 400 V were set as source parameters. The mass spectrometer was calibrated with an ES tuning mix from Agilent Technologies. Data was acquired with MassHunter Acquisition B.09.00 and analysed using MassHunter Qualitative analysis B.08.00 as software packages from Agilent Technologies, USA. Microanalyses were carried out in the analytical laboratories of the University of Eastern Finland and TU Dortmund.

Bis-(2-diphenylphosphino)phosphinic acid (***P*³*OO***H).

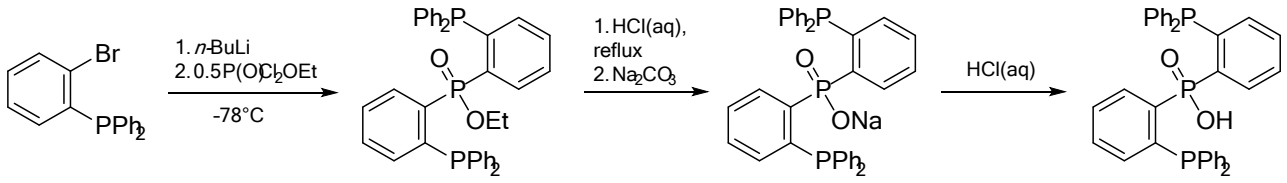

P*³*OOEt, 74% ***P*³*OO***Na, 95% ***P*³*OO***H, 92%

(2-Bromophenyl)diphenylphosphine (9.3 g, 27.2 mmol) was dissolved in freshly distilled THF (100 mL), cooled to –78 °C and a solution of *n*-BuLi in hexanes (1.6 M, 18.7 mL, 29.9 mmol) was added dropwise within 40 min. The reaction mixture was stirred below –70° C for 1 hour and treated dropwise with ethyl phosphorodichloridate (2.5 g, 15.5 mmol) to give dark orange-brown solution. It was slowly heated to room temperature and the solvents were removed in *vacuo*. The resulting oily

material of ethyl bis(2-(diphenylphosphaneyl)phenyl)phosphinate (***P*^{3}*OO*Et) was digested with methanol (10 ml) under ultrasonification to give white microcrystalline product, which was collected by filtration and dried (6.1 g, 74 %).

In the next step, the intermediate compound ***P*^{3}*OO*Et (3.9 g, 6.3 mmol) was treated with an excess of concentrated hydrochloric acid upon refluxing for 12 hours and then extracted with dichloromethane (40 ml). The combined organic layers were neutralized by aqueous solution of Na_2CO_3, leading to the precipitation of sodium bis(2-(diphenylphosphaneyl)phenyl)phosphinate (***P*^{3}*OO*Na), which was collected and washed with diethyl ether, acetone and dried (3.7 g, 95%). Subsequent treatment of a methanol solution (50 ml) of ***P*^{3}*OO*Na (513 mg, 0.8 mmol) with equimolar amount of hydrochloric acid (37 %, 110 µl) leads to the precipitation of bis(2-(diphenylphosphaneyl)phenyl)phosphinic acid (***P*^{3}*OO*H). It was collected, washed with water, methanol and dried under vacuum to give the pure ligand as a white microcrystalline solid (456 mg, 92%). Single crystals for the XRD structural analysis were obtained by a gas-phase diffusion of diethyl ether into a dichloromethane solution of **c** at –18º C. ^{1}H NMR (400 MHz, $CDCl_3$, 297 K; δ): 13.32 (s br, 1H), 8.35 (dddt, J_{PH} 11.3 Hz and 7.7 Hz, J_{HH} 3.4 Hz and 1.6 Hz, 2H), 7.36–7.42 (m, 2H), 7.29–7.37 (m, 6H), 7.20–7.29 (m, 10H), 7.09 (td, J_{PH} 7.7 Hz, J_{HH} 7.6 Hz and 1.3 Hz, 8H). ^{31}P{^{1}H} NMR (162 MHz, $CDCl_3$, 297 K; δ): 33.5 (t, $^3J_{PP}$ 11.3 Hz, 1P, P(O)OH), –14.5 (d, $^3J_{PP}$ 11.3 Hz, 2P, PPh_2).

[Ag$_2$(*P*^{3}*OO*)$_2$] (1). ***P*^{3}*OO*H (200 mg, 0.34 mmol) and silver phenylacetylenide AgC_2Ph (72 mg, 0.34 mmol) were suspended in dichloromethane (50 mL). The reaction mixture was stirred for 4 hours in the absence of light to give nearly transparent colorless solution. The solvent was evaporated *in vacuo*. The colorless residue was washed with diethyl ether (3×3 mL) under ultrasonification. The resulting solid was recrystallized by the slow evaporation of a methanol/acetonitrile solution at room temperature to give white crystalline material (157 mg, 67 %). ^{1}H NMR (400 MHz, CD_2Cl_2, 297 K; δ): 7.45 (m, 1H), 7.14–7.30 (m, 6H), 7.04–7.15 (m, 4H), 7.01–7.04 (m, 12H), 7.00 (m, 3H), 6.79–6.86 (m, 2H). ^{31}P{^{1}H} NMR (162 MHz, CD_2Cl_2, 297 K; δ): 25.9 (s br, 1P, P(O)O), 4.4 (d br, $^1J_{PAg}$ ca. 230 Hz, 1P, PPh_2), 2.9 (d br, $^1J_{PAg}$ ca. 230 Hz, 1P, PPh_2). ESI-MS (*m/z*): $[M+H]^+$ 1387.0783 (calcd 1387.0784). Anal. Calcd for $C_{72}H_{56}Ag_2O_4P_6 \cdot 4CH_3OH$: C, 60.25; H, 4.79. Found: C, 60.14; H, 4.34.

[Ag$_2$(*P*^{3}*OO*H)$_2$](CF$_3$SO$_3$)$_2$ (2). ***P*^{3}*OO*H (100 mg, 0.17 mmol) and $AgCF_3SO_3$ (44 mg, 0.17 mmol) were dissolved in tetrahydrofuran (20 mL) and stirred for 4 hours in the absence of light. The product partially precipitated from the reaction mixture. The solvent was evaporated in *vacuo* and the residue was treated with diethyl ether (2×5 mL) under ultrasonification. Recrystallization by cooling the saturated solution of crude **2** in dichloromethane/methanol/diethyl ether (4:1:8 v/v mixture, 13 ml) to

–18 ºC gave colorless crystalline material (113 mg, 79 %). Single crystals for the XRD structural analysis were obtained by a gas-phase diffusion of diethyl ether into a dichloromethane/methanol solution of **2** at room temperature. ^{1}H NMR (400 MHz, CD_2Cl_2, 193 K; δ): 15.33 (br, 1H), 8.00–7.75 (m, 4H), 7.66–6.76 (m, 42H), 6.67–6.10 (m, 8H), 5.69 (m, 2H). ^{31}P{^{1}H} NMR (162 MHz, CD_2Cl_2, 297 K; δ): 34.8 (m, 3P), 31.7 (m, 1P), 30.2 (d, J_{PP} 4.6 Hz, 1P), 28.9 (t, J_{PP} 4.6 Hz, 1P), 5.6–8.2 (m, 6P), –4.8–5.6 (m, 6P). ESI-MS (*m/z*): $[0.5M]^+$ 695.0455 (calcd 695.0427). Anal. Calcd for $C_{74}H_{58}Ag_2F_6O_{10}P_6S_2$: C, 52.69; H, 3.47. Found: C, 52.70; H, 3.66.

$[Ag_3(P^3OO)_3H]CF_3SO_3$ (3). ***P*^{3}*OO*H** (200 mg, 0.340 mmol), AgC_2Ph (48 mg, 0.227 mmol) and $AgCF_3SO_3$ (30 mg, 0.114 mmol) were suspended in dichloromethane (30 mL) and stirred for 2 hours in the absence of light to give nearly transparent colorless solution. The solvent was evaporated in *vacuo* and the residue was treated with diethyl ether (2×5 mL) under ultrasonification. The resulting solid was recrystallized by cooling its saturated solution in dichloromethane/diethyl ether (1:3 v/v mixture, 12 ml) to –18 ºC to give white crystalline material (115 mg, 91 %). Single crystals for the XRD structural analysis were obtained by slow evaporation of a chloroform/hexane solution of **3** at room temperature. ^{1}H NMR (400 MHz, CD_2Cl_2, 297 K; δ): 8.15–8.27 (m, 1H), 7.81–7.99 (m, 3H), 7.57–7.70 (m, 3H), 7.54 (d, J_{PH} 8.9 Hz, 2H), 7.38–7.50 (m, 2H), 7.12–7.39 (m, 15H), 7.07–7.12 (m, 4H), 6.96–7.07 (m, 10H), 6.88–6.96 (m, 13H), 6.79–6.88 (m, 4H), 6.69–6.78 (m, 6H), 6.66 (ddd, J_{PH} 16.0 Hz, J_{HH} 7.2 Hz and 2.1 Hz, 6H), 6.47–6.59 (m, 4H), 6.34–6.47 (m, 4H), 6.30–6.34 (m, 2H), 6.22–6.30 (m, 4H), 6.02 (ddq, J_{PH} 8.9 Hz, J_{HH} 7.5 Hz and 1.4 Hz, 1H), 5.90 (dddd, J_{PH} 13.5 Hz, J_{HH} 7.9 Hz, 4.3 and 1.4 Hz, 1H). ^{31}P{^{1}H} NMR (162 MHz, CD_2Cl_2, 293 K; δ): 31.5 (s, 1P), 30.1 (d, J_{PP} 4.4 Hz, 1P), 28.8 (t, J_{PP} 4.4 Hz, 1P), 6.1 to –5.7 (m, 6P). ESI-MS (*m/z*): $[M]^+$ 2081.1113 (calcd 2081.1163). Anal. Calcd for $C_{109}H_{85}Ag_3F_3O_9P_9S$: C, 58.70; H, 3.84. Found: C, 58.33; H, 3.74.

$[Au_2(P^3OH)_2]Cl_2$ (4). Bis-(2-diphenylphosphino)phosphine oxide H***P*$_3$*O*^{4} (100 mg, 0.175 mmol) and Au(tht)Cl (56 mg, 0.175 mmol) were dissolved in dichloromethane (10 mL) and stirred for 4 hours in the absence of light. The solvent was evaporated in *vacuo*. The residue was treated with diethyl ether (2×5 mL) under ultrasonification. The resulting solid was recrystallized by a gas-phase diffusion of diethyl ether into a dichloromethane solution of **4** at room temperature to give yellow crystals (115 mg, 82 %). ^{1}H NMR (500 MHz, CD_2Cl_2, 297 K; δ): 11.6 (v br, POH), 8.2-6.5 (br unresolved m). ^{31}P{^{1}H} NMR (202 MHz, CD_2Cl_2, 297 K; δ): 101.4 (br, 2P), 30.3 (br, 2P), 18.7 (br, 2P). Anal. Calcd for $C_{72}H_{58}Au_2Cl_2O_2P_6{\cdot}CH_2Cl_2$: C, 51.86; H, 3.58. Found: C, 51.75; H, 3.95.

[Au$_2$(*P*^{3}*OO*)$_2$H]CF$_3$SO$_3$ (5). Au(tht)Cl (100 mg, 0.312 mmol) was dissolved in dichloromethane (10 mL) and ***P*^{3}*OO*H** (183 mg, 0.312 mmol) was added. The colorless solution was stirred for 10 min. and treated with a solution of $AgCF_3SO_3$ (80 mg, 0.311 mmol) in acetonitrile (5 mL). The mixture was stirred for 1 h protected from light, then the precipitate of AgCl was filtered off, solvents were evaporated to give colorless amorphous residue. Recrystallization by a gas phase diffusion of diethyl ether into an acetone solution of crude **5** gave colorless crystalline material of an acetone solvate (235 mg, 88 %), suitable for single crystal XRD structural analysis. Alternatively, crystallization by a slow evaporation of an acetonitrile-water solution of **5** at room temperature afforded the product as a colorless acetonitrile solvate. ^{1}H NMR (400 MHz, CD_3CN, 233 K; δ): 18.23 (s, 1H), 6.23–8.26 (bm, 56H). ^{31}P{^{1}H} NMR (162 MHz, CD_3CN, 233 K; δ): ABX system 47.0 (d, $^2J_{PP}$ 365 Hz, 1P, PPh_2), 45.2 (d, $^2J_{PP}$ 365 Hz, 1P, PPh_2), 22.9 (s, 1P, P(O)OH). ESI-MS (*m/z*): $[M]^+$ 1565.1987 (calcd 1562.2008). Anal. Calcd for $C_{73}H_{57}Au_2F_3O_7P_6S$: C, 51.12; H, 3.35. Found: C, 51.03; H, 3.60.

[Au$_3$(*P*^{3}*O*)$_2$]CF$_3$SO$_3$ (6). Au(tht)Cl (21 mg, 0.066 mmol) and tetrahydrothiophene (3 drops) were dissolved in dichloromethane (5 mL) and a solution of $AgCF_3SO_3$ (17 mg, 0.0661 mmol) in methanol (3 mL). The mixture was stirred for 30 min. protected from light, then the precipitate of AgCl was filtered off, and a pale-yellow solution was added dropwise to a yellow-orange solution of [Au$_2$(***P*^{3}*O***)$_2$][5] (100 mg, 0.065 mmol) in dichloromethane-methanol 9:1 v/v mixture (10 ml) under a nitrogen atmosphere. The stirring continued for 1h, then the resulting dark yellow solution with perceptible green luminescence was filtered to remove a small amount of dark solid and evaporated. The amorphous yellow residue was washed with pentane (2×5 mL) under ultrasonification. Recrystallization by a gas-phase diffusion of pentane into an acetonitrile-diethyl ether solution of crude **6** afforded pale-yellow crystalline material with bright sky-blue luminescence (94 mg, 77 %). ^{1}H NMR (500 MHz, CD_2Cl_2, 297 K; δ): 8.16 (m, 2H), 7.66 (dd, $^3J_{HP}$ 13.1 Hz, $^2J_{HH}$ 7.3 Hz, 6H), 7.56–7.23 (m, 30 H), 7.20 (t, $^2J_{HH}$ 7.1 Hz, 2H), 7.10 (m, 6H), 7.03 (m, 2H), 6.88 (t, $^2J_{HH}$ 9.2 Hz, 2H), 6.54 (dd, $^3J_{HP}$ 11.4 Hz, $^2J_{HH}$ 7.8 Hz, 4H). ^{31}P{^{1}H} NMR (202 MHz, CD_2Cl_2, 297 K; δ): $X_2AA'BB'$ spin system 82.9 (J_{PP} XA 13 Hz, XA′ 12 Hz, XB 23 Hz, XA′ 25 Hz, 2P, PO), 38.0 (J_{PP} AB′ and A′B 324 Hz, AX 13 Hz, A′X 12 Hz, AA′ 1 Hz, 2P, PPh_2), 35.0 (J_{PP} BA′ and B′A 324 Hz, BX 23 Hz, B′X 25 Hz, BB′ 7 Hz, 2P, PPh_2). ESI-MS (*m/z*): $[M]^+$ 1729.27014 (calcd 1729.17031). Anal. Calcd for $C_{73}H_{56}Au_3F_3O_5P_6S$: C, 46.66; H, 3.00. Found: C, 46.42; H, 3.31.

Reaction of [Au$_2$(*P*^{3}*OH*)$_2$]Cl$_2$ (5) with AgCF$_3$SO$_3$. To a solution of complex **4** (75 mg, 0.047 mmol) in dichloromethane (7 mL) was added a solution of $AgCF_3SO_3$ (25 mg, 0.094 mmol) in acetone (2 mL) and the mixture was stirred on air for 30 min. The precipitate of AgCl was filtered off and the

solvents were evaporated. The residue was treated with diethyl ether (2×3 mL) under ultrasonification.It was dissolved in acetonitrile, diluted with water and left for a slow evaporation to give light yellow crystalline material (38 mg, 46 %) identified as **4** doped with a few percent of **6**s. ^{1}H NMR (400 MHz, CD_3CN, 233 K; δ): 18.23 (s, 1H), 6.23–8.26 (bm, 56H). ^{31}P{^{1}H} NMR (162 MHz, CD_3CN, 233 K; δ): ABX system 47.0 (d, $^{2}J_{PP}$ 365 Hz, 1P, PPh_2), 45.2 (d, $^{2}J_{PP}$ 365 Hz, 1P, PPh_2), 22.9 (s, 1P, P(O)OH). ESI-MS (*m/z*): $[M]^+$ 1565.1987 (calcd 1562.2008). Anal. Calcd for $C_{73}H_{57}Au_2F_3O_7P_6S{\cdot}C_3H_6O{\cdot}H_2O$: C, 50.96; H, 3.66. Found: C, 51.03; H, 3.90.

Reaction of [Ag$_2$(*P*^{3}*O*)$_2$] with CF$_3$SO$_3$H. A solution of [Ag$_2$(*P*^{3}*O*)$_2$] (15 mg, 0.011 mmol) in dichloromethane (5 mL) was treated with 5 equivalents of CF_3SO_3H dissolved in methanol (1 mL) and the mixture was stirred on air for 30 min. The solvents were evaporated. The residue was treated with water (2×1 mL) under ultrasonification. The resulting solid was recrystallized by a gas-phase diffusion of diethyl ether into a dichloromethane/methanol (4:1 v/v mixture) solution at room temperature to give colorless crystalline material (11 mg, 59 %) identified as **2**.

Reaction of [Au$_2$(*P*^{3}*O*)$_2$] with CF$_3$SO$_3$H. A solution of [Au$_2$(*P*^{3}*O*)$_2$] (15 mg, 0.010 mmol) in dichloromethane (5 mL) was treated with 5 equivalents of CF_3SO_3H dissolved in acetonitrile (1 mL) and the mixture was stirred on air for 30 min to give a solution with bright green luminescence. The solvents were evaporated. The residue was treated with water (2×1 mL) under ultrasonification. The resulting solid was dissolved in acetonitrile, diluted with water and left for a slow evaporation to give light yellow crystalline material (9 mg, 52 %) showing sky-blue luminescence and identified as **5** doped with 1–2% of **6**.

X-ray Structure Determination. The crystals of *P*^{3}*OO*H, **1**–**6** were immersed in cryo oil, mounted in a Nylon loop, and measured at a temperature of 150 K. The diffraction data were collected with Bruker SMART APEX II, Kappa Apex II, Kappa Apex II Duo, Rigaku Super Nova and Synergy S diffractometers using Mo Kα (λ = 0.71073 Å) and Cu Kα (λ = 1.5184 Å) radiation. The APEX2[6] and CrysAlisPro[7] program packages were used for cell refinements and data reductions. The structures were solved by direct methods using the SHELXS-2018[8] programs with the WinGX[9] and Olex2[10] graphical user interface. A semiempirical or numeric absorption correction (SADABS[11] or CrysAlisPro[7]) was applied to all data. Structural refinements were carried out using SHELXL-2017/2019.[8]

Some of the partially lost solvent molecules were refined with partial occupancy (0.25 for water in **1**(X/H_2O); 0.5 for acetone in **5***; 0.5 for diethyl ether in **6** (diethyl ether solvate); 0.5 and 0.25 for water in **6** (acetonitrile solvate)).

The OOP-C_6H_4 group and two phenyl rings in **1**(X/H_2O) were modeled as disordered between two positions each and refined with occupancies of 0.71/0.29, 0.73/0.27, and 0.70/030. The structure of **5**+**6** 2:1 mixture was refined with partial occupancies of O(3)···H(1)···O(4) (66.7%) and Au(1) (33.3%) components corresponding to compounds **5** and **6**. The $CF_3SO_3^-$ counterion was disordered between two orientations and was modeled with occupancies of 0.38/0.62.

The crystallization solvent in **1**(X/H_2O), **3**, **5** (acetonitrile solvate), **6** (diethyl ether solvate) was lost/disordered and could not be reliably determined. The contribution of missing solvent to the calculated structure factors was taken into account by using a SQUEEZE and BYPASS routines of PLATON[12] and Olex2, respectively,[10] and was not included in the unit cell content.

The positions of H_2O hydrogen atoms in **1**(X/H_2O) were estimated with CALC-OH program,[13] the O···H···O hydrogen atoms in **3**, **5**, **5*** and **5**+**6** (2:1 mixture) were located from the difference Fourier map and constrained to ride on the parent atoms, with U_{iso} = 1.2–1.5 U_{eq} (parent atom). All other H atoms in **1**–**6** were positioned geometrically and constrained to ride on their parent atoms C–H = 0.95–0.99 Å, O–H = 0.84 and U_{iso} = 1.2–1.5 U_{eq} (parent atom). The crystallographic details are summarized in Table S1.

Photophysical Measurements. Both excitation and emission spectra of the samples were recorded on an Edinburgh Instrument FLS1000 spectrometer, equipped with a 450 W ozone-free Xenon arc lamp, double monochromators for the excitation and emission pathways, and a red-sensitive photomultiplier (PMT-980, 200-880 nm) as detector. Solutions of the **4** were prepared in the glovebox at 0.1 A at the excitation wavelength and approx. at concentration of 10^{-5} M, using solvents from purification system PureSolv MD 7, which were additionally degassed by freeze-pump-thaw technique. Absorption spectra were recorded on an Agilent Cary 5000 UV-Vis-NIR spectrophotometer (175–3300 nm range). The excitation and emission spectra were corrected using the standard corrections supplied by the manufacturer for the spectral power of the excitation source and the sensitivity of the detector. The solid state absorptance spectra at 297 K ($BaSO_4$ used as a reflectance reference standard) and quantum yields in range of 77 K–297 K were measured by use of an Oxford Microstat integrating cryosphere linked to an Edinburgh Instrument FLS1000 spectrometer by two fibre bundles. The luminescence lifetimes were measured using a pulsed 60 W Xenon microsecond flashlamp, with a repetition rate of 1-100 Hz, or LED pulsed laser diodes (365, 380, 450 nm) with a multichannel scaling (MCS) or Time-Correlated Single Photon Counting (TCSPC)

modules. The emission was collected at right angles to the excitation source with the emission wavelength selected using a double grated monochromator and detected by the respective PMT. Steady-state and time-resolved low temperature measurements were performed utilizing an Oxford Optistat DN cryostate. Origin Pro 2019 9.6.0, Cary WinUV, Fluoracle and FAST spectrometer operating software were used for data analysis and processing.

DFT calculations. DFT and TD-DFT calculations for complexes **1**, $\mathbf{2}^{2+}$, $\mathbf{5}^{+}$ and $\mathbf{6}^{+}$ were performed with the ORCA 6.0.1 program suite with tight SCF convergence criteria.[14] Geometry optimizations (gas-phase) omitting the respective anions were carried out with the BP86 functional[15] as implemented in ORCA, and a frequency analysis ensuring that the optimized structures correspond to energy minima. The def2-SVP[16] basis set was used for all atoms together with the auxiliary basis set SARC/J[17-21] in order to accelerate the computations within the framework of RI approximation. Relativistic effects were accounted for by employing the ZORA method as implemented for the def2-SVP basis set in Orca, and by employing the SARC-ZORA-TZVP[19, 22] basis set for the metal atoms. Van der Waals interactions have been considered by an empirical dispersion correction (Grimme-D3BJ).[23, 24] TD-DFT calculations for the first 20 singlet and triplet excited states of **1**, $\mathbf{2}^{2+}$, $\mathbf{5}^{+}$ and $\mathbf{6}^{+}$ were performed with the same basis sets, but the PBE0 functional[25, 26] was used. Representations of electronic transition differences at isovalues of 0.0005 were produced with orca_plot as provided by ORCA 6.0.1 and with Chimera.[27]

Table S1. Crystal data and structure refinement for **1**–**6** and ***P³OO***H.

Identification code	**1**	**1**(MeOH)	**1**(X/H_2O)
CCDC	2475264	2475266	2475265
Empirical formula	$C_{72}H_{56}Ag_2O_4P_6$	$C_{80}H_{88}Ag_2O_{12}P_6$	$C_{72}H_{57}Ag_2O_{4.5}P_6$
Formula weight	1386.72	1643.06	1395.73
T (K)		150(2)	
λ (Å)		0.71073	
Crystal system	Triclinic	Triclinic	Triclinic
Space group	$P\bar{1}$	$P\bar{1}$	$P\bar{1}$
Unit cell dimensions			
a (Å)	11.2019(7)	12.0333(9)	12.1097(5)
b (Å)	12.2462(7)	13.0167(10)	12.2400(4)
c (Å)	12.8767(8)	14.1395(11)	13.4687(6)
α (deg)	62.205(2)	86.506(3)	97.831(3)
β (deg)	70.808(2)	67.479(3)	112.619(4)
γ (deg)	73.368(2)	67.237(2)	111.980(4)
Volume ($Å^3$)	1456.98(16)	1876.6(3)	1614.72(13)
Z	1	1	1
ρ_{calc} (Mg/m^3)	1.580	1.454	1.435
μ (mm^{-1})	0.890	0.711	0.804
F(000)	704	848	709
Crystal size (mm^3)	0.407×0.308×0.277	0.425×0.329×0.294	0.108×0.066×0.045
θ range for data collection (deg.)	1.837 to 27.996	1.994 to 29.999	2.444 to 30.374
Index ranges	-14≤h≤14, -16≤k≤16, -17≤l≤16	-16≤h≤16, -18≤k≤16, -19≤l≤19	-16≤h≤16, -16≤k≤16, -18≤l≤19
Reflections collected	34185	42610	15794
Unique reflections	7021	10864	8550
R_{int}	0.0251	0.0193	0.0237
Completeness to θ= 25.242°	99.9 %	99.7 %	99.9 %
Absorption correction	semi-empirical from equivalents		numerical
Max. and min. transmission	0.791 and 0.713	0.818 and 0.752	1.000 and 0.911
Refinement method	Full-matrix least-squares on F^2		
Data / restraints / parameters	7021 / 0 / 379	10864 / 10 / 458	8550 / 57 / 484
GOOF on F^2	1.040	1.076	1.027
Final R indices	R_1 = 0.0276, wR_2 =	R_1 = 0.0318, wR_2 =	R_1 = 0.0393, wR_2 =

[I>2sigma(I)][a]	0.0690	0.0875	0.0790
R indices (all data)	R_1 = 0.0325, wR_2 = 0.0717	R_1 = 0.0350, wR_2 = 0.0902	R_1 = 0.0559, wR_2 = 0.0867
Largest diff. peak and hole (e.Å^{-3})	1.779 and -0.611	1.74 and -1.67	0.809 and -0.888

[a] $R_1 = \Sigma||F_o| - |F_c||/\Sigma|F_o|$; $wR_2 = [\Sigma[w(F_o^2 - F_c^2)^2]/ \Sigma[w(F_o^2)^2]]^{1/2}$

Table S1. Continued.

Identification code	**2**	**3**	**4**
CCDC	2475267	2475268	2475269
Empirical formula	$C_{74}H_{58}Ag_2F_6O_{10}P_6S_2$	$C_{119}H_{99}Ag_3Cl_{21}F_3O_9P_9S$	$C_{75}H_{64}Au_2Cl_8O_2P_6$
Formula weight	1686.88	3108.83	1860.61
T (K)		150(2)	
λ (Å)		0.71073	
Crystal system	Triclinic	Triclinic	Monoclinic
Space group	$P\bar{1}$	$P\bar{1}$	$P2_1/n$
Unit cell dimensions			
a (Å)	12.5845(10)	13.6740(7)	23.0253(10)
b (Å)	12.8489(10)	22.7670(12)	20.6697(10)
c (Å)	12.9550(10)	23.8565(13)	34.6257(15)
α (deg)	99.025(3)	62.068(2)	90
β (deg)	114.193(3)	79.031(2)	108.1770(10)
γ (deg)	108.723(3)	86.638(2)	90
Volume (Å^3)	1705.9(2)	6437.8(6)	15656.9(12)
Z	1	2	8
ρ_{calc} (Mg/m^3)	1.642	1.604	1.579
μ (mm^{-1})	0.854	1.075	4.182
F(000)	852	3122	7312
Crystal size (mm^3)	0.140×0.133×0.129	0.365×0.279×0.114	0.360×0.134×0.049
θ range for data collection (deg.)	1.775 to 25.998	1.649 to 27.545	0.943 to 26.000
Index ranges	-15≤h≤15, -15≤k≤15, -15≤l≤15	-17≤h≤17, -28≤k≤24, -29≤l≤30	-28≤h≤28, -25≤k≤25, -42≤l≤42
Reflections collected	38818	83765	168755
Unique reflections	6698	28577	30799
R_{int}	0.0503	0.0485	0.1186
Completeness to θ= 25.242°	100.0 %	99.8 %	100.0 %

Absorption correction	semi-empirical from equivalents		numerical
Max. and min. transmission	0.898 and 0.890	0.887 and 0.695	0.821 and 0.314
Refinement method	Full-matrix least-squares on F^2		
Data / restraints / parameters	6698 / 6 / 452	28577 / 12 / 1351	30799 / 12 / 1679
GOOF on F^2	1.068	1.025	1.097
Final R indices [I>2sigma(I)][a]	R_1 = 0.0587, wR_2 = 0.1497	R_1 = 0.0631, wR_2 = 0.1602	R_1 = 0.0701, wR_2 = 0.1381
R indices (all data)	R_1 = 0.0787, wR_2 = 0.1607	R_1 = 0.0995, wR_2 = 0.1783	R_1 = 0.1197, wR_2 = 0.1537
Largest diff. peak and hole (e.Å^{-3})	2.075 and -0.591	2.030 and -1.201	5.599 and -1.822

[a] $R_1 = \Sigma||F_o| - |F_c||/\Sigma|F_o|$; $wR_2 = [\Sigma[w(F_o^2 - F_c^2)^2]/ \Sigma[w(F_o^2)^2]]^{1/2}$.

Table S1. Continued.

Identification code	**5* (acetone solvate)**	**5 (acetonitrile solvate)**	**5+6 2:1 mixture**
CCDC	2475270	2475271	2475274
Empirical formula	$C_{79}H_{69}Au_2F_3O_9P_6S$	$C_{79}H_{66}Au_2F_3N_3O_7P_6S$	$C_{80}H_{67.67}Au_{2.33}Cl_2F_3N_3O_{6.33}P_6S$
Formula weight	1831.15	1838.16	1977.56
T (K)		150(2)	
λ (Å)	0.71073	1.54184	1.54184
Crystal system	Monoclinic	Monoclinic	Monoclinic
Space group	$P2_1/c$	$P2_1/c$	$P2_1/c$
Unit cell dimensions			
a (Å)	14.2851(13)	14.38860(10)	14.46810(10)
b (Å)	26.190(2)	26.3090(2)	26.1628(2)
c (Å)	20.8252(19)	20.55300(10)	20.76600(10)
α (deg)	90	90	90
β (deg)	94.625(2)	96.6330(10)	96.2550(10)
γ (deg)	90	90	90
Volume (Å^3)	7765.8(12)	7728.25(9)	7813.68(9)
Z	4	4	4
ρ_{calc} (Mg/m^3)	1.566	1.580	1.681
μ (mm^{-1})	3.986	8.972	10.645
F(000)	3624	3632	3882
Crystal size (mm^3)	0.254×0.209×0.108	0.223×0.045×0.026	0.431×0.097×0.056
θ range for data collection (deg.)	2.113 to 26.000	2.740 to 80.161	2.727 to 80.183

Index ranges	-17≤h≤17, -32≤k≤32, -25≤l≤25	-18≤h≤18, -33≤k≤33, -25≤l≤18	-18≤h≤18, -31≤k≤32, -23≤l≤26
Reflections collected	72221	79381	77052
Unique reflections	15231	16398	16650
R_{int}	0.0573	0.0353	0.0422
Completeness to θ= 25.242°/67.684°	99.7 %	99.9 %	99.9 %
Absorption correction	numerical		
Max. and min. transmission	0.673 and 0.431	0.853 and 0.205	1.000 and 0.518
Refinement method	Full-matrix least-squares on F^2		
Data / restraints / parameters	15231 / 118 / 937	16398 / 0 / 913	16650 / 61 / 1022
GOOF on F^2	1.028	1.049	1.088
Final R indices [I>2sigma(I)][a]	R_1 = 0.0358, wR_2 = 0.0777	R_1 = 0.0338, wR_2 = 0.0890	R_1 = 0.0462, wR_2 = 0.1148
R indices (all data)	R_1 = 0.0566, wR_2 = 08	R_1 = 0.0378, wR_2 = 0.0911	R_1 = 0.0483, wR_2 = 0.1161
Largest diff. peak and hole (e.$Å^{-3}$)	1.353 and -0.606	1.690 and -2.085	2.313 and -1.410

[a] $R_1 = \Sigma||F_o| - |F_c||/\Sigma|F_o|$; $wR_2 = [\Sigma[w(F_o^2 - F_c^2)^2]/ \Sigma[w(F_o^2)^2]]^{1/2}$.

Table S1. Continued.

Identification code	**6 (diethyl ether solvate)**	**6 (acetonitrile solvate)**	***P*^{3}*OO*H**
CCDC	2475272	2475273	2475275
Empirical formula	$C_{150}H_{122}Au_6F_6O_{11}P_{12}S_2$	$C_{316}H_{270}Au_{12}F_{12}N_{12}O_{25}P_{24}S_4$	$C_{36}H_{29}O_2P_3$
Formula weight	3832.03	8098.54	586.50
T (K)	150(2)		
λ (Å)	1.54184	1.54184	0.71073
Crystal system	Orthorhombic	Orthorhombic	Triclinic
Space group	*Pbca*	*Pbca*	$P\bar{1}$
Unit cell dimensions			
a (Å)	25.0213(3)	24.87400(10)	9.2537(5)
b (Å)	23.7785(3)	23.95100(10)	11.5109(7)
c (Å)	25.5290(3)	25.32280(10)	15.2834(9)
α (deg)	90	90	95.663(2)
β (deg)	90	90	94.800(2)

γ (deg)	90	90	109.560(2)
Volume (Å^3)	15189.0(3)	15189.0(3)	1514.66(15)
Z	4	2	2
ρ_{calc} (Mg/m^3)	1.676	1.783	1.286
μ (mm^{-1})	12.583	12.727	0.228
F(000)	7400	7860	612
Crystal size (mm^3)	0.208×0.162×0.010	0.256×0.163×0.155	0.295×0.237×0.214
θ range for data collection (deg.)	3.094 to 80.298	3.491 to 80.104	3.354 to 35.043
Index ranges	-16≤≤h≤31, -28≤k≤30, -30≤l≤32	-31≤h≤29, -30≤k≤20, -25≤l≤32	-14≤h≤14, -16≤k≤17, -23≤l≤22
Reflections collected	68115	72272	38971
Unique reflections	16087	16106	11710
R_{int}	0.0487	0.0428	0.0349
Completeness to θ= 25.242°/67.684°	99.8 %	100.0 %	99.8 %
Absorption correction	numerical		
Max. and min. transmission	1.000 and 0.511	0.499 and 0.150	0.953 and 0.936
Refinement method	Full-matrix least-squares on F^2		
Data / restraints / parameters	16087 / 6 / 867	16106 / 12 / 930	11710 / 0 / 371
GOOF on F^2	1.083	1.064	1.036
Final R indices [I>2sigma(I)][a]	R_1 = 0.0587, wR_2 = 0.1448	R_1 = 0.0346, wR_2 = 0.0917	R_1 = 0.0440, wR_2 = 0.1000
R indices (all data)	R_1 = 0.0679, wR_2 = 0.1504	R_1 = 0.0373, wR_2 = 0.0934	R_1 = 0.0708, wR_2 = 0.1116
Largest diff. peak and hole (e.Å^{-3})	2.511 and -1.719	1.302 and -0.892	0.475 and -0.322

[a] $R_1 = \Sigma||F_o| - |F_c||/\Sigma|F_o|$; $wR_2 = [\Sigma[w(F_o^2 - F_c^2)^2]/ \Sigma[w(F_o^2)^2]]^{1/2}$.

Table S2. Selected bond lengths (Å) and angles (º) for ***P³OO*H.

	Bond length, Å		**Bond angle, º**
P(2)–C(1)	1.8258(15)	O(1)-P(1)-C(18)	109.65(5)
P(2)–C(7)	1.8335(14)	O(1)-P(1)-C(19)	110.14(5)
P(2)–C(13)	1.8458(12)	O(1)-P(1)-O(2)	114.54(5)
P(1)–C(18)	1.8019(12)	O(2)-P(1)-C(18)	104.25(5)
P(1)–C(19)	1.8031(13)	O(2)-P(1)-C(19)	107.74(5)
P(3)–C(24)	1.8470(11)		
P(3)–C(25)	1.8346(13)		
P(3)–C(31)	1.8283(14)		
P(1)–O(1)	1.4973(9)		
P(1)–O(2)	1.5505(9)		
O(2)···O(1′)	2.551(1)		

Table S3. Selected bond lengths (Å) angles (º) for complex **1**(MeOH).

	Bond length, Å		**Bond angles, º**
Ag(1)–O(1)	2.3611(13)	O(1)-Ag(1)-P(2)	138.24(3)
Ag(1)–O(1)'	2.4990(13)	O(1)-Ag(1)-P(3)	83.63(3)
Ag(1)–P(2)'	2.3994(4)	P(2)-Ag(1)-P(3)	138.115(16)
Ag(1)–P(3)	2.4378(5)	O(1)-Ag(1)-O(1)'	80.12(5)
Ag(1)'–O(1)	2.4990(13)	P(2)-Ag(1)-O(1)'	80.30(3)
O(1)–P(1)	1.4988(13)	P(3)-Ag(1)-O(1)'	114.04(3)
O(2)–P(1)	1.5038(14)	Ag(1)-O(1)-Ag(1)'	99.88(5)
		P(1)-O(1)-Ag(1)'	135.91(7)
		P(1)-O(1)-Ag(1)	123.57(7)

Table S4 Selected bond lengths (Å) and angles (º) for complex **1**(X/H_2O) (major component).

	Bond length, Å		**Bond angle, º**
Ag(1)–O(1)	2.446(3)	O(1)-Ag(1)-P(2)	129.36(8)
Ag(1)–O(2)	2.466(3)	O(2)-Ag(1)-P(3)	143.38(6)
Ag(1)–P(2)	2.4640(8)	P(2)-Ag(1)-P(3)	128.43(3)
Ag(1)–P(3)	2.4416(7)	O(2)-Ag(1)-O(1)	100.30(10)
O(1)–P(1′)	1.501(3)	P(1′)-O(1)-Ag(1)'	129.99(17)
O(2)–P(1)	1.503(3)	P(1)-O(2)-Ag(1)	97.27(15)

Table S5. Selected bond lengths (Å) and angles (º) for complex **1**.

	Bond length, Å		**Bond angle, º**
Ag(1)–O(1)	2.4615(14)	P(2)-Ag(1)-P(3)'	130.033(17)
Ag(1)–O(2)'	2.4552(14)	P(2)-Ag(1)-O(2)'	137.17(4)
Ag(1)–P(2)	2.4338(5)	P(3)'-Ag(1)-O(2)'	91.36(4)
Ag(1)–P(3)'	2.4517(5)	P(2)-Ag(1)-O(1)	70.71(3)
O(1)–P(1)	1.4979(14)	P(3)'-Ag(1)-O(1)	128.14(3)
O(2)–P(1)	1.5056(14)	O(2)'-Ag(1)-O(1)	93.60(5)
		P(1)-O(1)-Ag(1)	124.89(8)
		P(1)-O(2)-Ag(1)'	97.47(7)

Table S6. Selected bond lengths (Å) and angles (º) for complex **2**.

	Bond length, Å		**Bond angle, º**
Ag(1)–O(1)	2.396(3)	O(1)-Ag(1)-O(1)'	75.51(12)
Ag(1)–O(1)'	2.547(3)	O(1)-Ag(1)-P(2)	87.36(8)
Ag(1)–P(2)	2.4390(12)	O(1)-Ag(1)-P(3)'	139.81(9)
Ag(1)–P(3)'	2.4137(12)	P(2)-Ag(1)-O(1)'	147.77(9)
O(1)–P(1)	1.482(3)	P(3)'-Ag(1)-O(1)'	76.09(8)
O(2)–P(1)	1.555(3)	P(3)'-Ag(1)-P(2)	130.21(4)
O(2)···O(4´)	2.565(7)	Ag(1)-O(1)-Ag(1)'	104.49(12)
		P(1)-O(1)-Ag(1)	119.19(18)
		P(1)-O(1)-Ag(1)'	136.31(19)

Table S7. Selected bond lengths (Å) and angles (º) for complex **3**.

	Bond length, Å		**Bond angle, º**
Ag(1)–O(1)	2.352(3)	O(1)-Ag(1)-P(5)	145.26(9)
Ag(1)–P(5)	2.3823(13)	O(1)-Ag(1)-P(2)	85.49(9)
Ag(1)–P(2)	2.4356(14)	P(5)-Ag(1)-P(2)	128.97(5)
Ag(1)–O(3)	2.522(4)	O(1)-Ag(1)-O(3)	88.17(11)
Ag(2)–O(4)	2.266(3)	P(5)-Ag(1)-O(3)	74.15(9)
Ag(2)–O(5)	2.330(3)	P(2)-Ag(1)-O(3)	127.95(9)
Ag(2)–P(3)	2.3669(14)	O(4)-Ag(2)-O(5)	88.05(13)
Ag(2)–O(1)	2.533(3)	O(4)-Ag(2)-P(3)	143.73(10)
Ag(3)–P(6)	2.4416(14)	O(5)-Ag(2)-P(3)	122.11(9)
Ag(3)–P(8)	2.4969(14)	O(4)-Ag(2)-O(1)	113.46(12)
Ag(3)–P(9)	2.4974(14)	O(5)-Ag(2)-O(1)	85.71(12)
O(1)–P(1)	1.494(3)	P(3)-Ag(2)-O(1)	90.34(8)
O(2)–P(1)	1.521(3)	P(6)-Ag(3)-P(8)	119.19(5)
O(3)–P(4)	1.479(4)	P(6)-Ag(3)-P(9)	125.98(5)
O(4)–P(4)	1.517(4)	P(8)-Ag(3)-P(9)	102.76(5)
O(5)–P(7)	1.486(4)	P(1)-O(1)-Ag(1)	113.51(19)
O(6)–P(7)	1.531(4)	P(1)-O(1)-Ag(2)	112.76(17)
O(6)···O(2)	2.445(7)	Ag(1)-O(1)-Ag(2)	98.14(12)
		P(1)-O(2)-H(2A)	127.4
		P(4)-O(3)-Ag(1)	127.3(2)
		P(4)-O(4)-Ag(2)	112.7(2)
		P(7)-O(5)-Ag(2)	133.0(2)
		P(7)-O(6)-H(2A)	129.8
		O(1)-P(1)-O(2)	115.4(2)
		O(3)-P(4)-O(4)	118.5(2)
		O(5)-P(7)-O(6)	116.7(2)

Table S8. Selected bond lengths (Å) and angles (º) for complex **4** (the data correspond to two independent molecules found in the unit cell).

	Bond length, Å		**Bond angle, º**
Au(1)-P(1)	2.321(3)	P(1)-Au(1)-P(4)	144.61(10)
Au(1)-P(4)	2.380(3)	P(1)-Au(1)-P(3)	87.08(10)
Au(1)-P(3)	2.426(3)	P(4)-Au(1)-P(3)	103.04(10)
Au(1)-P(6)	2.485(3)	P(1)-Au(1)-P(6)	126.38(10)
Au(1)-Au(2)	2.8615(6)	P(4)-Au(1)-P(6)	80.37(10)
Au(2)-P(5)	2.301(3)	P(3)-Au(1)-P(6)	114.61(10)
Au(2)-P(2)	2.341(3)	P(1)-Au(1)-Au(2)	75.20(7)
Au(3)-P(10)	2.384(3)	P(4)-Au(1)-Au(2)	79.85(7)
Au(3)-P(7)	2.320(3)	P(3)-Au(1)-Au(2)	149.71(7)
Au(3)-P(12)	2.488(3)	P(6)-Au(1)-Au(2)	95.65(7)
Au(3)-P(9)	2.418(3)	P(5)-Au(2)-P(2)	139.27(10)
Au(3)-Au(4)	2.8226(6)	P(5)-Au(2)-Au(1)	114.75(8)
Au(4)-P(8)	2.329(3)	P(2)-Au(2)-Au(1)	105.97(7)
Au(4)-P(11)	2.300(3)	P(10)-Au(3)-P(7)	145.94(10)
O(1)-P(1)	1.593(8)	P(10)-Au(3)-P(12)	80.58(9)
O(2)-P(4)	1.595(8)	P(7)-Au(3)-P(12)	125.33(10)
O(3)-P(7)	1.594(7)	P(10)-Au(3)-P(9)	100.92(10)
O(4)-P(10)	1.597(8)	P(7)-Au(3)-P(9)	87.80(10)
O(1)···Cl(1)	2.880(9)	P(12)-Au(3)-P(9)	115.46(9)
O(2)···Cl(2)	2.926(7)	P(10)-Au(3)-Au(4)	81.54(7)
O(3)···Cl(3)	2.855(9)	P(7)-Au(3)-Au(4)	74.87(7)
O(4)···Cl(4)	2.894(7)	P(12)-Au(3)-Au(4)	95.41(6)
		P(9)-Au(3)-Au(4)	149.08(7)
		P(8)-Au(4)-P(11)	137.88(10)
		P(8)-Au(4)-Au(3)	108.73(7)
		P(11)-Au(4)-Au(3)	113.24(7)
		O(1)-P(1)-Au(1)	124.3(3)
		O(2)-P(4)-Au(1)	104.5(3)
		O(3)-P(7)-Au(3)	124.4(3)
		O(4)-P(10)-Au(3)	105.2(3)

Table S9. Selected bond lengths (Å) and angles (º) for complexes **5** (acetonitrile solvate) / **5*** (acetone solvate).

	Bond length, Å		**Bond angle, º**
Au(2)–P(6)	2.2886(9)/ 2.3023(14)	P(5)-Au(1)-P(2)	172.48(3)/ 171.13(5)
Au(1)–P(2)	2.2934(8)/ 2.3196(12)	P(3)-Au(2)-P(6)	176.32(3)/ 176.71(5)
Au(2)–P(3)	2.2985(9)/ 2.2923(13)	O(2)-P(1)-O(1)	118.14(16)/ 117.4(2)
Au(1)–P(5)	2.3158(8)/ 2.2974(13)	O(4)-P(4)-O(3)	117.74(16)/ 118.4(2)
O(1)–P(1)	1.513(3)/ 1.535(3)		
O(2)–P(1)	1.482(3)/ 1.479(3)		
O(3)–P(4)	1.532(3)/ 1.520(4)		
O(4)–P(4)	1.480(3)/ 1.490(4)		
O(3)···O(1)	2.396(4)/ 2.391(5)		

Table S10. Selected bond lengths (Å) and angles (º) for complex **6** (diethyl ether/acetonitrile solvate).

	Bond length, Å		**Bond angle, º**
Au(1)-P(1)	2.315(2)/ 2.3175(11)	P(1)-Au(1)-P(4)	168.47(8)/ 167.69(4)
Au(1)-P(4)	2.321(2)/ 2.3239(11)	P(5)-Au(2)-P(2)	171.34(8)/ 173.03(4)
Au(1)-Au(2)	2.8414(5)/ 2.8695(2)	P(6)-Au(3)-P(3)	173.23(8)/ 172.16(4)
Au(1)-Au(3)	2.8568(5)/ 2.8676(2)	Au(2)-Au(1)-Au(3)	142.205(17)/ 144.772(8)
Au(2)-P(5)	2.313(2)/ 2.3178(11)		
Au(2)-P(2)	2.315(2)/ 2.3239(11)		
Au(3)-P(6)	2.320(2)/ 2.3162(11)		
Au(3)-P(3)	2.320(2)/ 2.3165(11)		
O(1)-P(1)	1.505(7)/ 1.518(3)		
O(2)-P(4)	1.498(7)/ 1.510(3)		

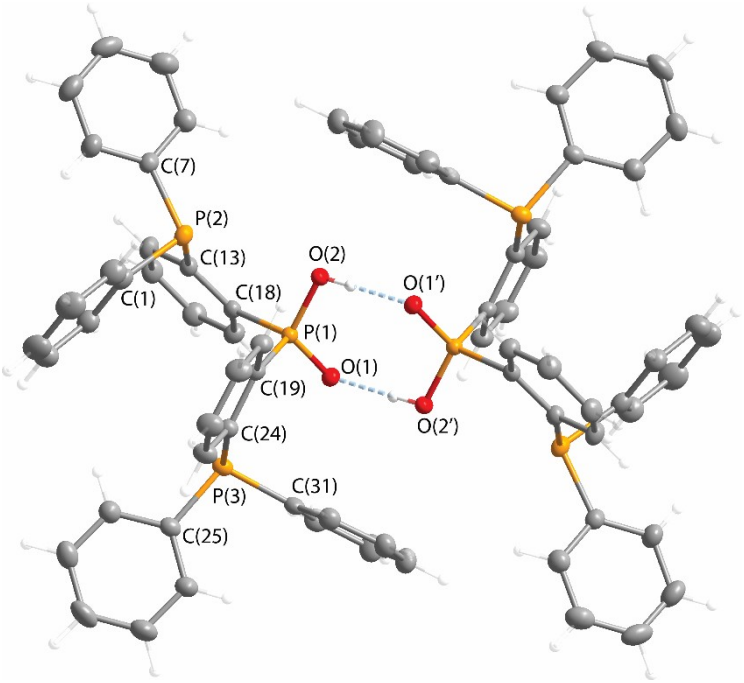

Fig. S1. Molecular view of hydrogen-bonded dimer of ***P³OO***H (displacement ellipsoids are shown at the 50% probability level).

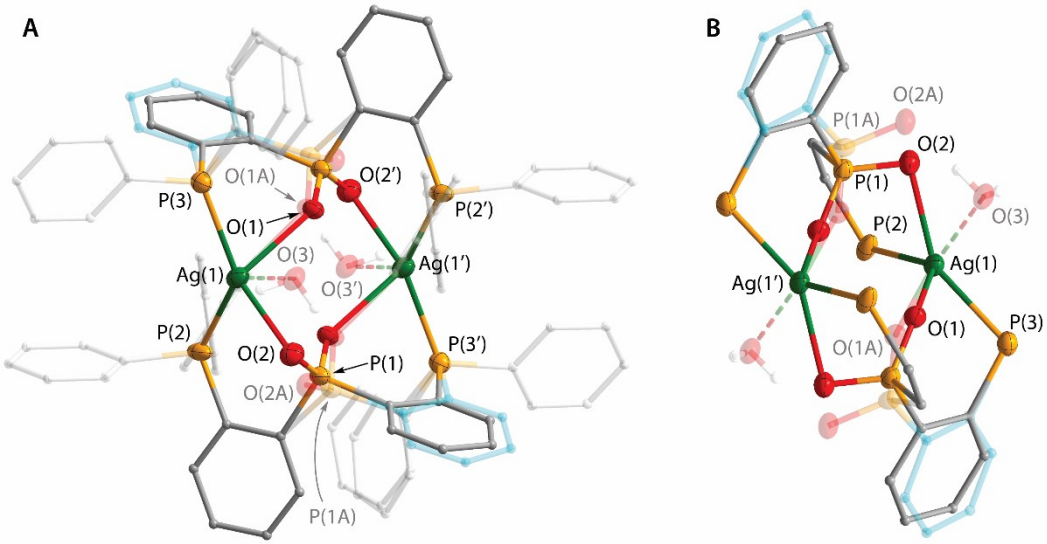

Fig. S2. Molecular views of **1**(X/H_2O) modification (displacement ellipsoids of non-carbon atoms are shown at the 50% probability level, hydrogen atoms are omitted for clarity). Disordered solvent X could not be resolved. Water molecule was refined with 0.25 occupancy. View (B) highlights a disorder of the POO^- group and phenylene spacer (second component at 0.27 occupancy is shown in semi-transparent mode).

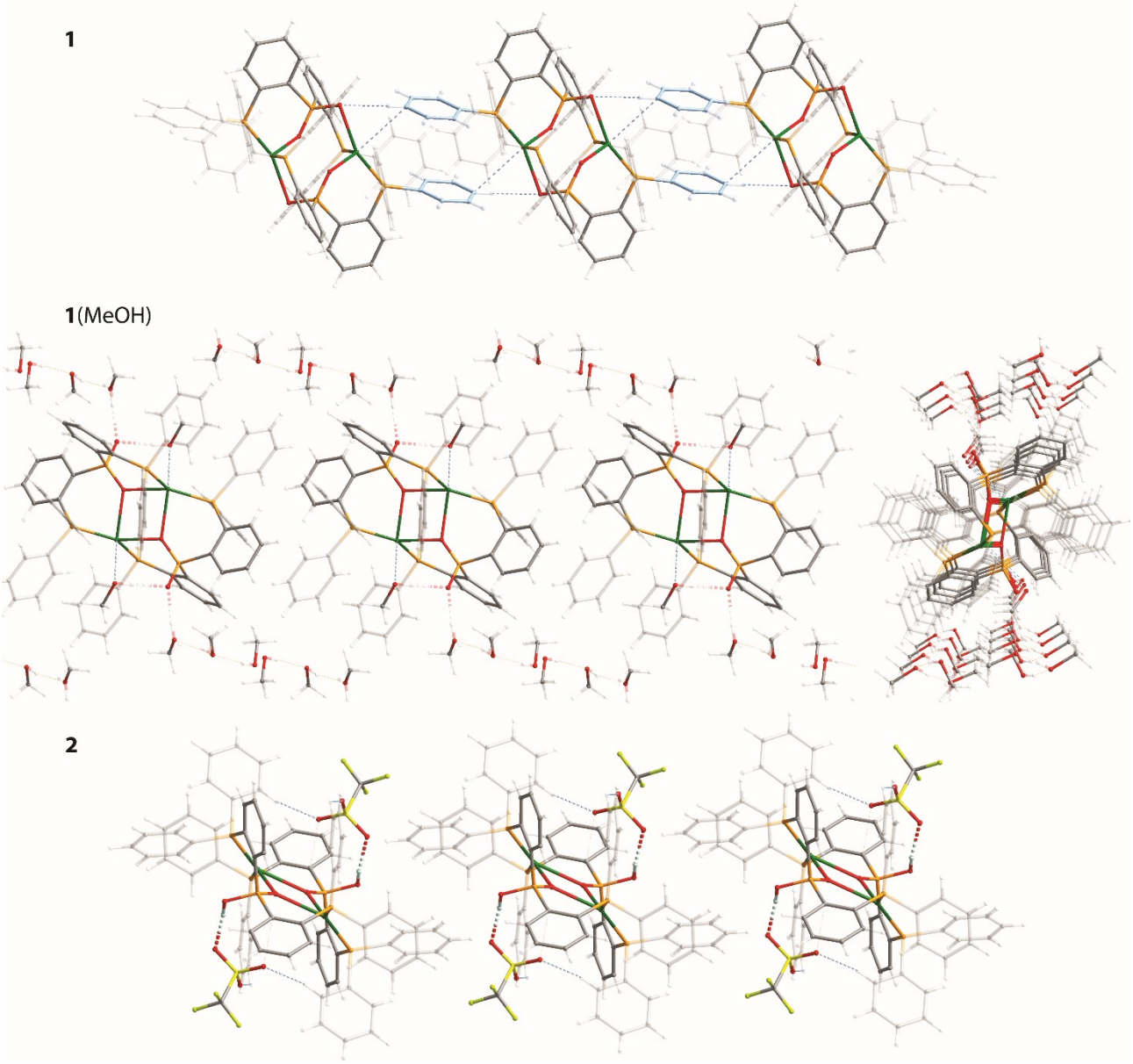

Fig. S3. Fragments of crystal packing of complexes **1**, **1**(MeOH) and **2**.

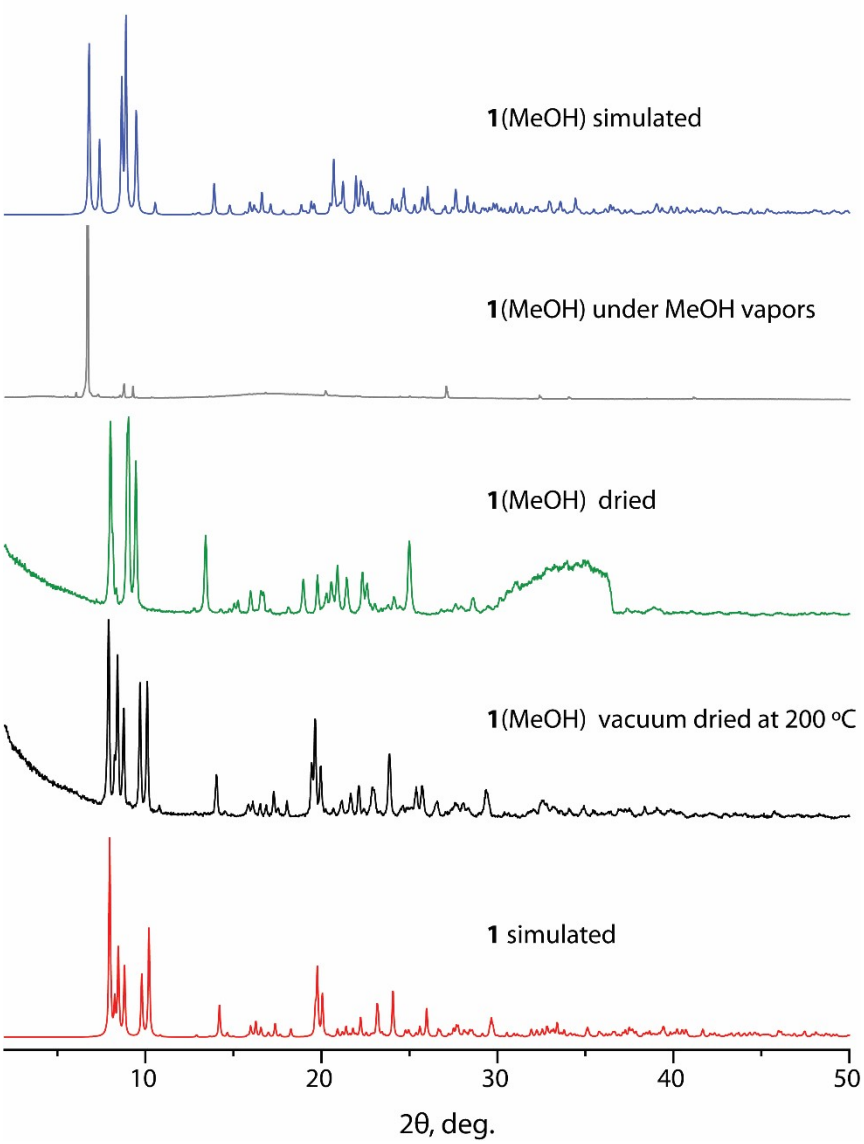

Fig. S4. Simulated and experimental powder X-ray diffraction patterns for **1**(MeOH) and solvent free forms of complex **1**.

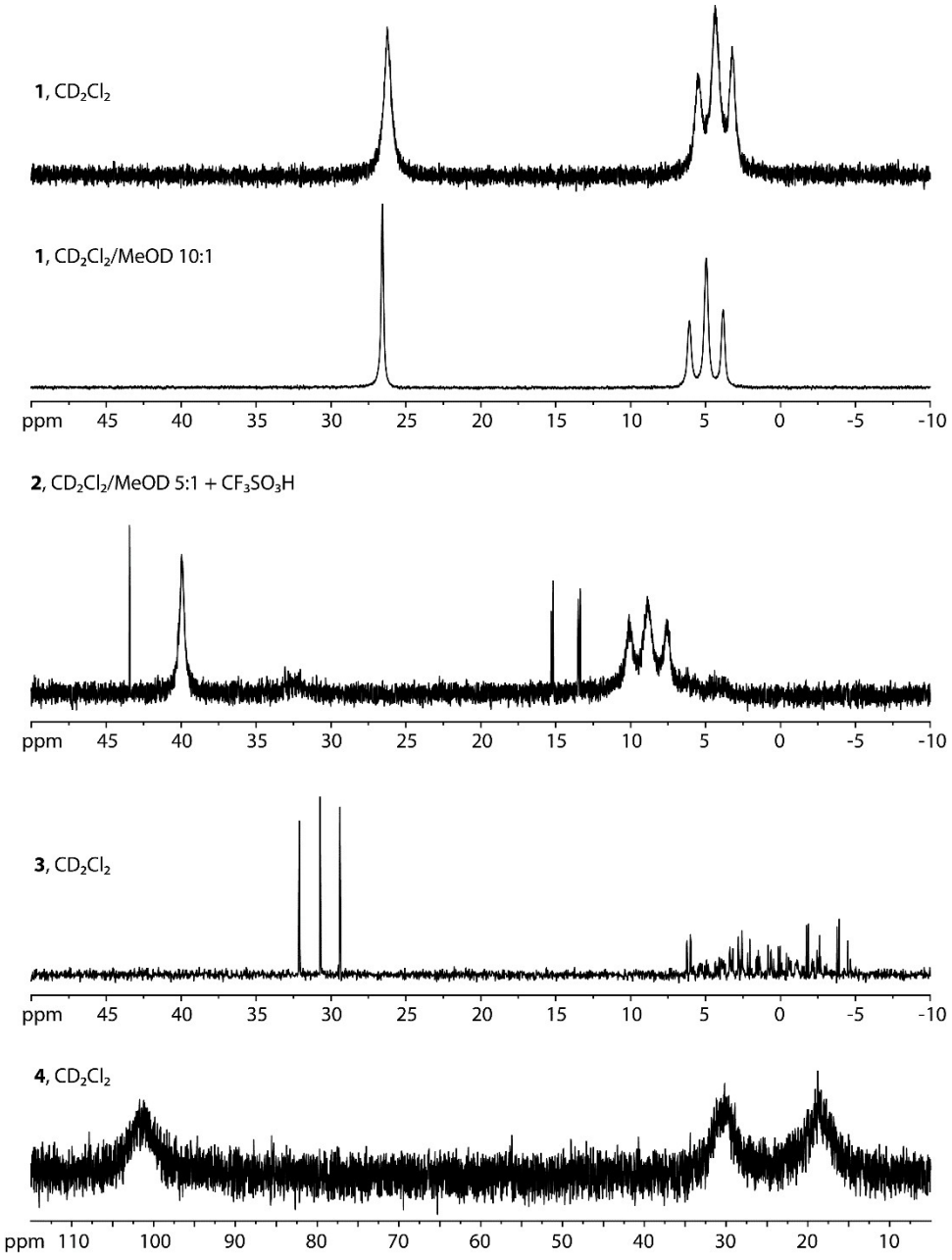

Fig. S5. 202 MHz $^{31}P\{^{1}H\}$ NMR spectra of complexes **1**–**4** (297 K).

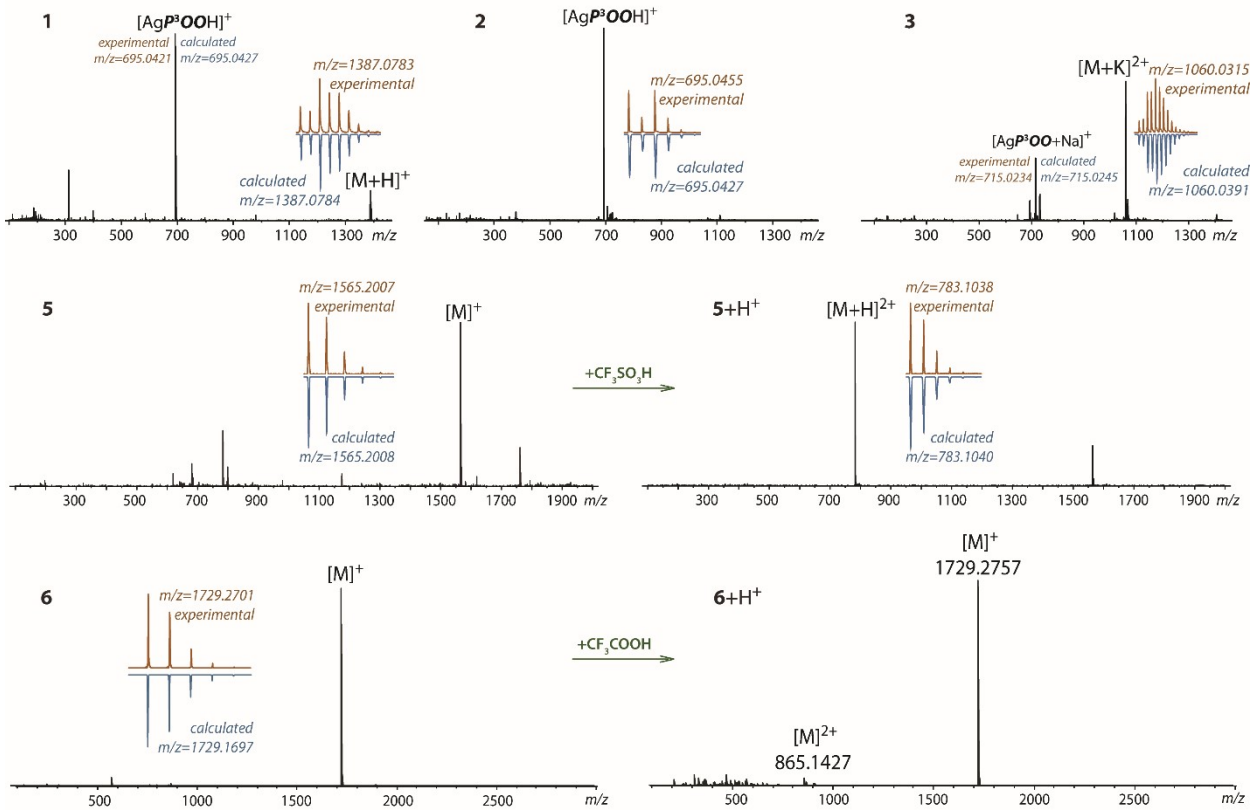

Fig. S6. ESI⁺-MS of compounds **1**–**5** (MeOH/acetonitrile 1:1 v/v) and **6** (acetonitrile).

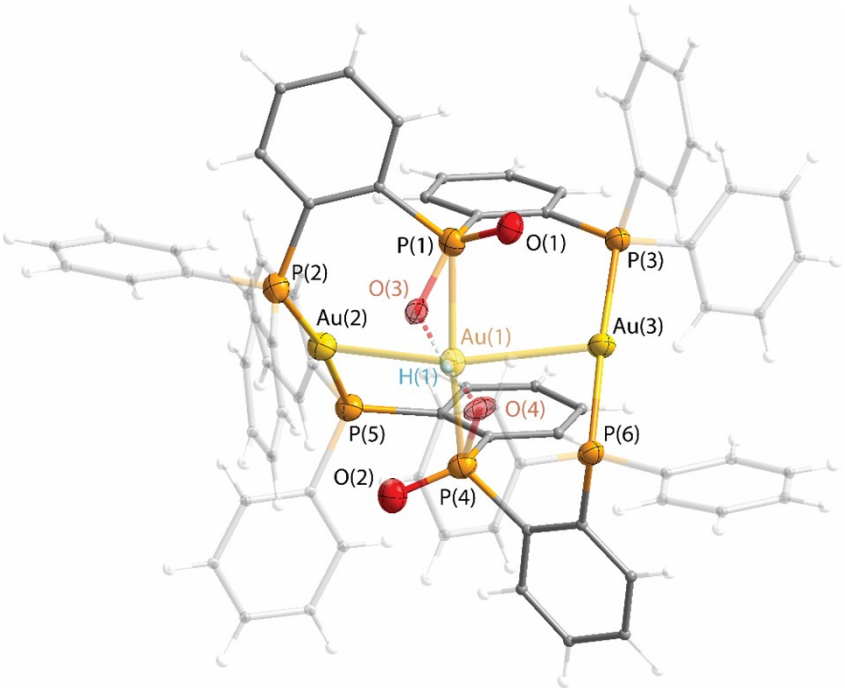

Fig. S7. Molecular view of co-crystallized **5** and **6** refined as a 2:1 mixture (66.7% of the O(3)···H(1)···O(4) component (**5**) and 33.3% of the Au(1) component (**6**); displacement ellipsoids of non-carbon atoms are shown at the 50% probability level).

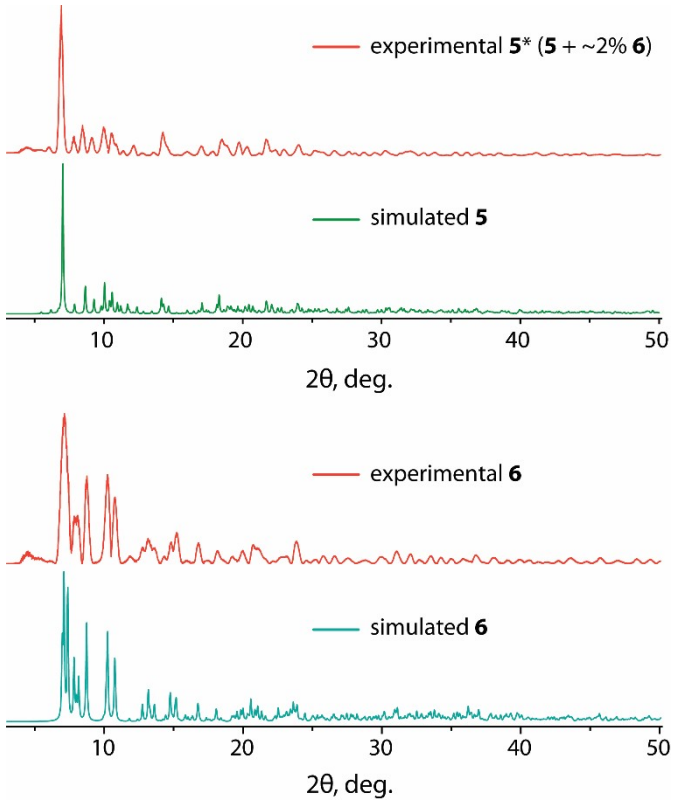

Fig. S8. Simulated and experimental powder X-ray diffraction patterns for **5*** (**5** doped with **6** ca. 2%) and **6**.

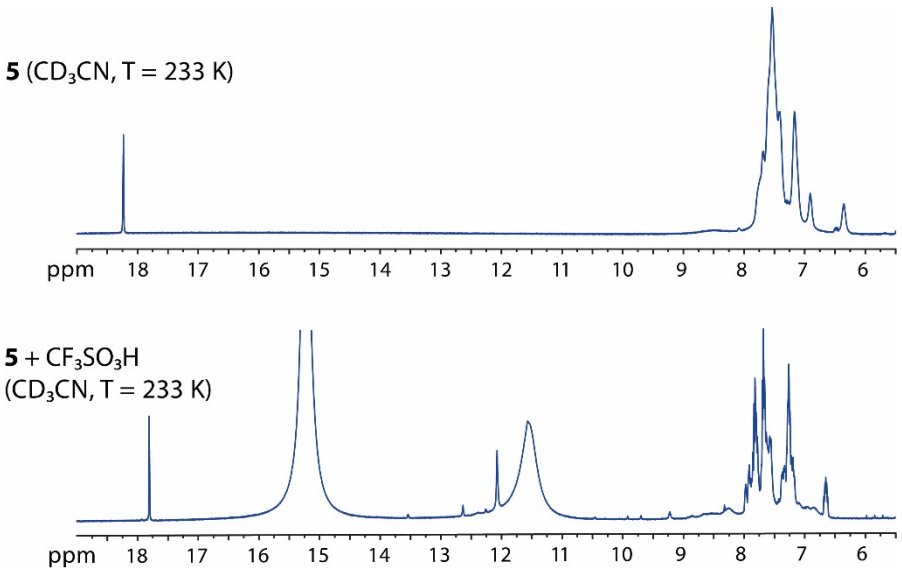

Fig. S9. ^{1}H NMR spectra of complex **5** before (top) and after (bottom) addition of excess of triflic acid.

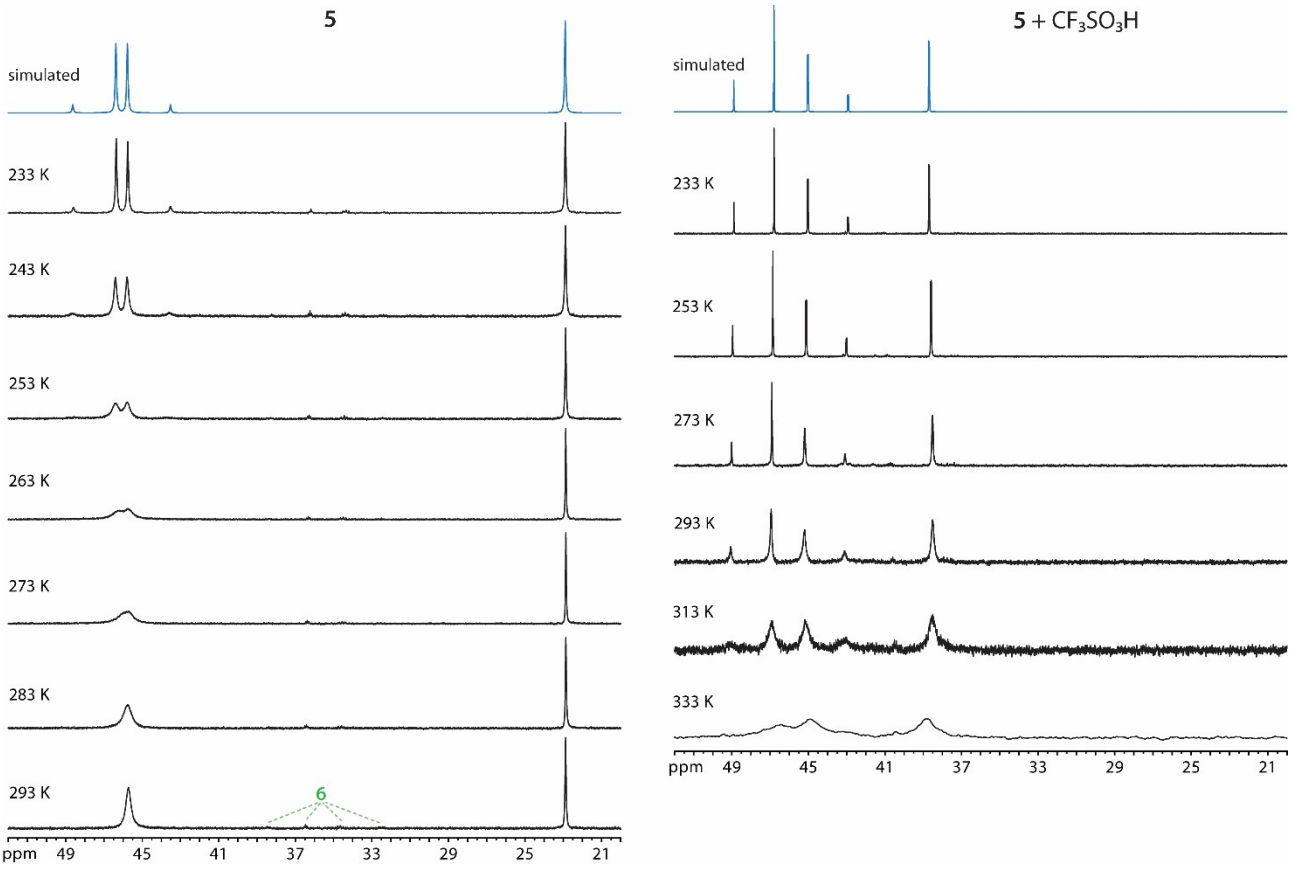

Fig. S10. Variable temperature 162 MHz $^{31}P\{^{1}H\}$ NMR spectra of compound **5*** before (left) and after (right) addition of excess of triflic acid (acetonitrile-d_3).

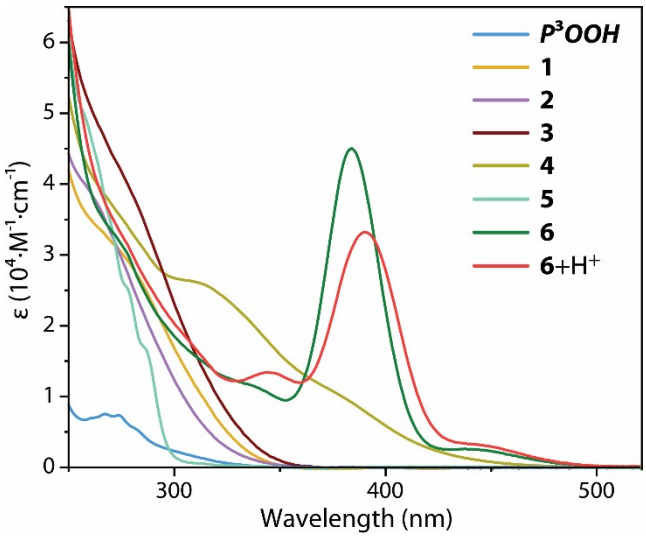

Fig. S11. UV-vis absorption spectra of **1**–**4**, **6**, **6**+H^+ and ***P*^{3}*OO*H (dichloromethane, 297 K).

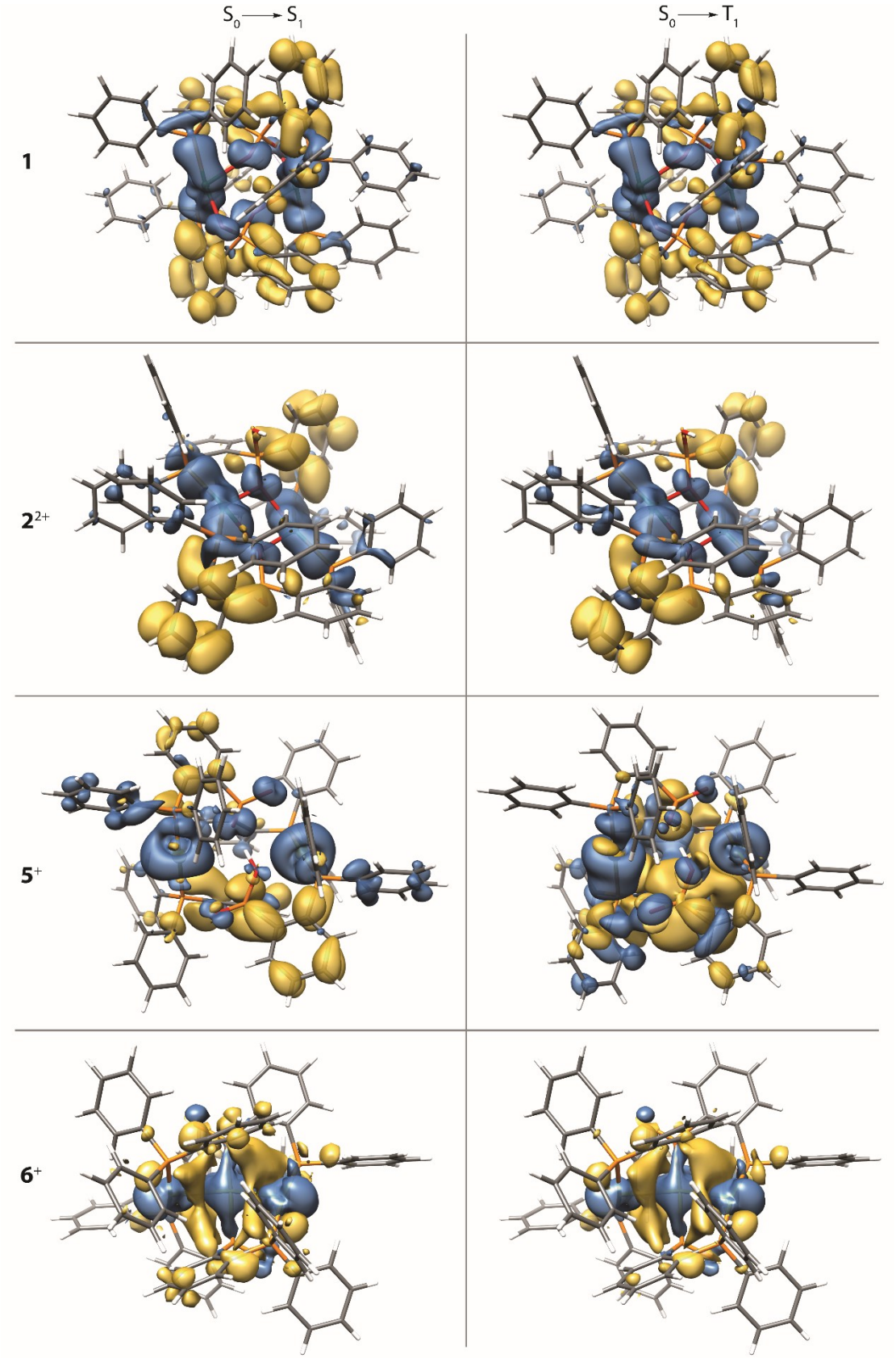

Fig. S12. Comparison of TD-DFT calculated transition density differences for vertical excitation from the DFT optimized ground state S_0 to the S_1 (left) and T_1 (right) excited states for **1**, $\mathbf{2}^{2+}$, $\mathbf{5}^{+}$ and $\mathbf{6}^{+}$. Loss of electron density shown in blue, gain in yellow. Anions have been omitted for calculations.

Table S11. TD-DFT calculated vertical electronic transitions from the ground state S_0 at the geometry of the DFT optimized ground state S_0 and triplet state T_1 of **1** to the first 10 and 5 singlet and triplet excited states, respectively.

Transition	Energy, eV	Energy, cm^{-1}	Wavelength, nm	Oscillator strength f
		S_0 geometry		
$S_0 \rightarrow S_1$	3.543939	28583.8	349.8	0.0000
$S_0 \rightarrow S_2$	3.571005	28802.1	347.2	0.0100
$S_0 \rightarrow S_3$	3.69662	29815.3	335.4	0.0186
$S_0 \rightarrow S_4$	3.720813	30010.4	333.2	0.0000
$S_0 \rightarrow S_5$	3.893236	31401.1	318.5	0.0672
$S_0 \rightarrow S_6$	3.897293	31433.8	318.1	0.0077
$S_0 \rightarrow S_7$	3.929819	31696.1	315.5	0.0858
$S_0 \rightarrow S_8$	3.945994	31826.6	314.2	0.0082
$S_0 \rightarrow S_9$	3.950146	31860.1	313.9	0.0002
$S_0 \rightarrow S_{10}$	3.967599	32000.8	312.5	0.0000
$S_0 \rightarrow T_1$	3.402585	27443.7	364.4	
$S_0 \rightarrow T_2$	3.418404	27571.3	362.7	
$S_0 \rightarrow T_3$	3.475765	28033.9	356.7	
$S_0 \rightarrow T_4$	3.477728	28049.8	356.5	
$S_0 \rightarrow T_5$	3.496681	28202.6	354.6	
$S_0 \rightarrow T_6$	3.49941	28224.7	354.3	
$S_0 \rightarrow T_7$	3.652652	29460.6	339.4	
$S_0 \rightarrow T_8$	3.657407	29499	339	
$S_0 \rightarrow T_9$	3.720177	30005.3	333.3	
$S_0 \rightarrow T_{10}$	3.721586	30016.6	333.1	
		T_1 geometry		
$S_0 \rightarrow S_1$	2.090841	16863.8	593	0.0160
$S_0 \rightarrow S_2$	2.246052	18115.6	552	0.0053
$S_0 \rightarrow S_3$	2.512923	20268.1	493.4	0.0055
$S_0 \rightarrow S_4$	2.5831	20834.1	480	0.0001
$S_0 \rightarrow S_5$	2.667193	21512.4	464.8	0.0071
$S_0 \rightarrow T_1$	1.906076	15373.5	650.5	
$S_0 \rightarrow T_2$	2.159631	17418.6	574.1	
$S_0 \rightarrow T_3$	2.449851	19759.4	506.1	
$S_0 \rightarrow T_4$	2.538707	20476.1	488.4	
$S_0 \rightarrow T_5$	2.580059	20809.6	480.5	

Table S12. TD-DFT calculated vertical electronic transitions from the DFT optimized ground state S_0 of $\mathbf{2}^{2+}$ to the first 10 singlet and triplet excited states.

Transition	Energy, eV	Energy, cm^{-1}	Wavelength, nm	Oscillator strength f
$S_0 \rightarrow S_1$	3.831297	30901.5	323.6	0.0000
$S_0 \rightarrow S_2$	3.911722	31550.2	317.0	0.0857
$S_0 \rightarrow S_3$	4.043918	32616.4	306.6	0.0291
$S_0 \rightarrow S_4$	4.107844	33132	301.8	0.0000
$S_0 \rightarrow S_5$	4.220341	34039.4	293.8	0.0095
$S_0 \rightarrow S_6$	4.266188	34409.1	290.6	0.0000
$S_0 \rightarrow S_7$	4.276734	34494.2	289.9	0.0312
$S_0 \rightarrow S_8$	4.324774	34881.7	286.7	0.0000
$S_0 \rightarrow S_9$	4.371025	35254.7	283.7	0.0000
$S_0 \rightarrow S_{10}$	4.415449	35613	280.8	0.1195
$S_0 \rightarrow T_1$	3.619891	29196.4	342.5	
$S_0 \rightarrow T_2$	3.648431	29426.6	339.8	
$S_0 \rightarrow T_3$	3.745528	30209.7	331.0	
$S_0 \rightarrow T_4$	3.765075	30367.4	329.3	
$S_0 \rightarrow T_5$	3.821327	30821.1	324.5	
$S_0 \rightarrow T_6$	3.83259	30911.9	323.5	
$S_0 \rightarrow T_7$	3.933904	31729.1	315.2	
$S_0 \rightarrow T_8$	3.94874	31848.7	314.0	
$S_0 \rightarrow T_9$	3.978247	32086.7	311.7	
$S_0 \rightarrow T_{10}$	3.978848	32091.6	311.6	

Table S13. TD-DFT calculated vertical electronic transitions from the DFT optimized ground state S_0 of $\mathbf{5}^+$ to the first 10 singlet and triplet excited states.

Transition	Energy, eV	Energy, cm^{-1}	Wavelength, nm	Oscillator strength f
$S_0 \rightarrow S_1$	4.470523	36057	277.3	0.0817
$S_0 \rightarrow S_2$	4.480441	36137	276.7	0.0236
$S_0 \rightarrow S_3$	4.530283	36539	273.7	0.2933
$S_0 \rightarrow S_4$	4.561032	36787	271.8	0.0087
$S_0 \rightarrow S_5$	4.592276	37039	270.0	0.0033
$S_0 \rightarrow S_6$	4.670386	37669	265.5	0.0341
$S_0 \rightarrow S_7$	4.706342	37959	263.4	0.0268
$S_0 \rightarrow S_8$	4.745521	38275	261.3	0.0188
$S_0 \rightarrow S_9$	4.764243	38426	260.2	0.0266
$S_0 \rightarrow S_{10}$	4.788544	38622	258.9	0.0899
$S_0 \rightarrow T_1$	3.694997	29802	335.5	
$S_0 \rightarrow T_2$	3.727109	30061	332.7	
$S_0 \rightarrow T_3$	3.762321	30345	329.5	
$S_0 \rightarrow T_4$	3.768520	30395	329.0	
$S_0 \rightarrow T_5$	3.851466	31064	321.9	
$S_0 \rightarrow T_6$	3.852458	31072	321.8	
$S_0 \rightarrow T_7$	3.853450	31080	321.7	
$S_0 \rightarrow T_8$	3.858657	31122	321.3	
$S_0 \rightarrow T_9$	3.873907	31245	320.1	
$S_0 \rightarrow T_{10}$	3.902796	31478	317.7	

Table S14. TD-DFT calculated vertical electronic transitions from the DFT optimized ground state S_0 of $\mathbf{6}^+$ to the first 10 singlet and triplet excited states.

Transition	Energy, eV	Energy, cm^{-1}	Wavelength, nm	Oscillator strength f
$S_0 \rightarrow S_1$	3.18957	25726	388.7	0.5088
$S_0 \rightarrow S_2$	3.27992	26454	378.0	0.0013
$S_0 \rightarrow S_3$	3.450943	27834	359.3	0.0210
$S_0 \rightarrow S_4$	3.536861	28527	350.5	0.0253
$S_0 \rightarrow S_5$	3.588773	28945	345.5	0.0509
$S_0 \rightarrow S_6$	3.689599	29759	336.0	0.0644
$S_0 \rightarrow S_7$	3.769843	30406	328.9	0.0569
$S_0 \rightarrow S_8$	3.824451	30846	324.2	0.0078
$S_0 \rightarrow S_9$	3.864567	31170	320.8	0.0405
$S_0 \rightarrow S_{10}$	3.880835	31301	319.5	0.0277
$S_0 \rightarrow T_1$	2.788198	22488.3	444.7	
$S_0 \rightarrow T_2$	3.091411	24933.9	401.1	
$S_0 \rightarrow T_3$	3.292939	26559.3	376.5	
$S_0 \rightarrow T_4$	3.333829	26889.1	371.9	
$S_0 \rightarrow T_5$	3.423875	27615.4	362.1	
$S_0 \rightarrow T_6$	3.492133	28166	355	
$S_0 \rightarrow T_7$	3.613216	29142.6	343.1	
$S_0 \rightarrow T_8$	3.623175	29222.9	342.2	
$S_0 \rightarrow T_9$	3.658965	29511.5	338.9	
$S_0 \rightarrow T_{10}$	3.678348	29667.9	337.1	

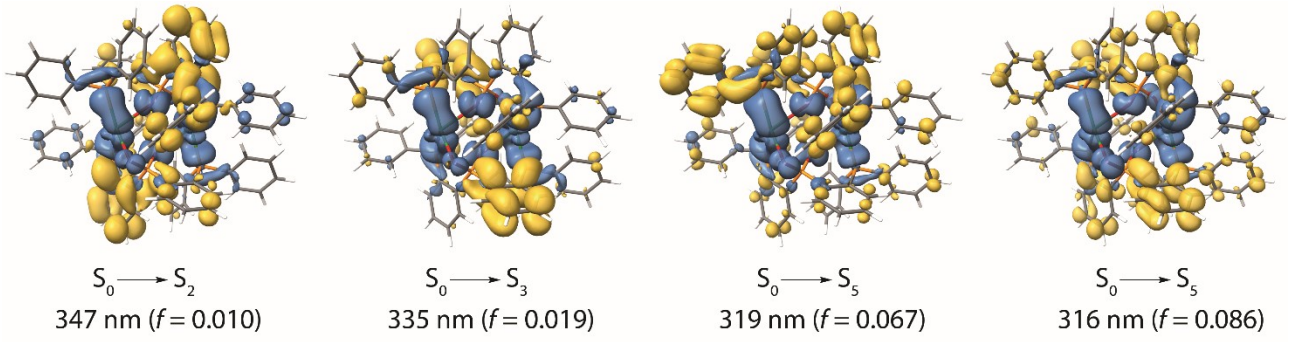

Fig. S13. TD-DFT calculated transition density differences of selected vertical excitations from the DFT-optimized ground state S_0 relevant for the observed experimental absorption spectrum for compound **1**.

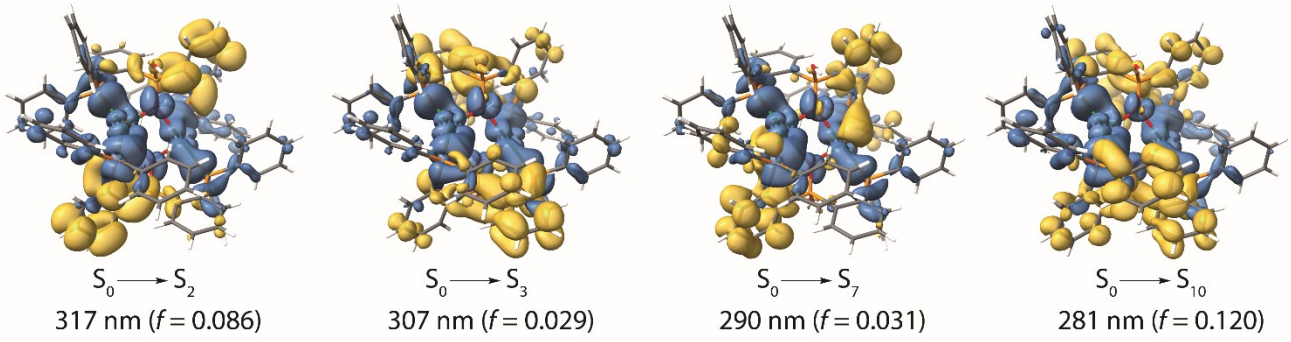

Fig. S14. TD-DFT calculated transition density differences of selected vertical excitations from the DFT-optimized ground state S_0 relevant for the observed experimental absorption spectrum for compound $\mathbf{2}^{2+}$.

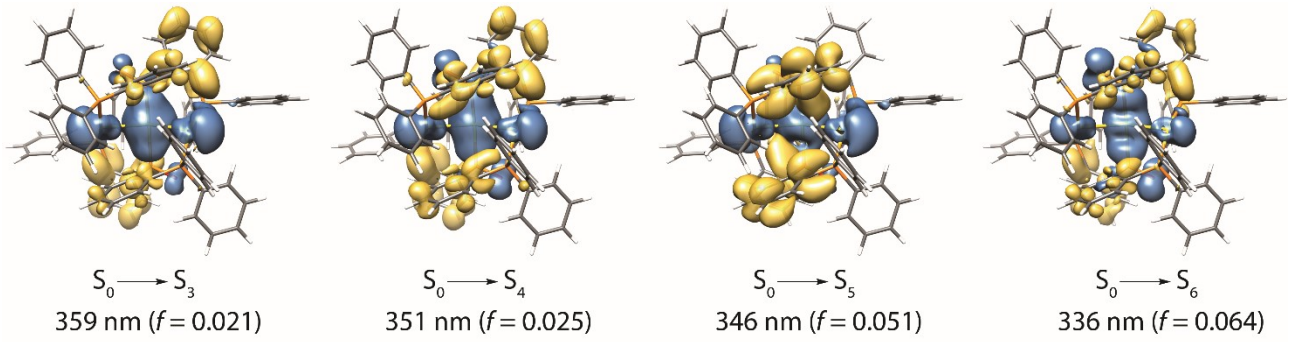

Fig. S15. TD-DFT calculated transition density differences of selected vertical excitations from the DFT-optimized ground state S_0 relevant for the observed experimental absorption spectrum for compound $\mathbf{6}^{+}$.

Table S15. Photophysical properties of **6** and **6**+H^+ in solution (dichloromethane, 297 K).

compound	λ_{abs}, nm (ε, 10^3 $M^{-1}{\cdot}cm^{-1}$)	λ_{em}, nm	τ_{obs}, μs[a]	Φ_{em}[a]	k_r, 10^5 s^{-1} [b]	k_{nr}, 10^5 s^{-1} [c]
6	277sh (30.6), 338sh (11.4), 384 (45.0), 440 (2.6)	500	-	0.004	-	-
6+H^+	277sh (31.8), 344 (13.4), 390 (33.2), 450 (2.9)	512	4.01	0.709	1.77	0.73

[a] oxygen-free conditions; [b] $k_r = \Phi_{em}/\tau_{obs}$; [c] $k_{nr} = (1 - \Phi_{em})/\tau_{obs}$.

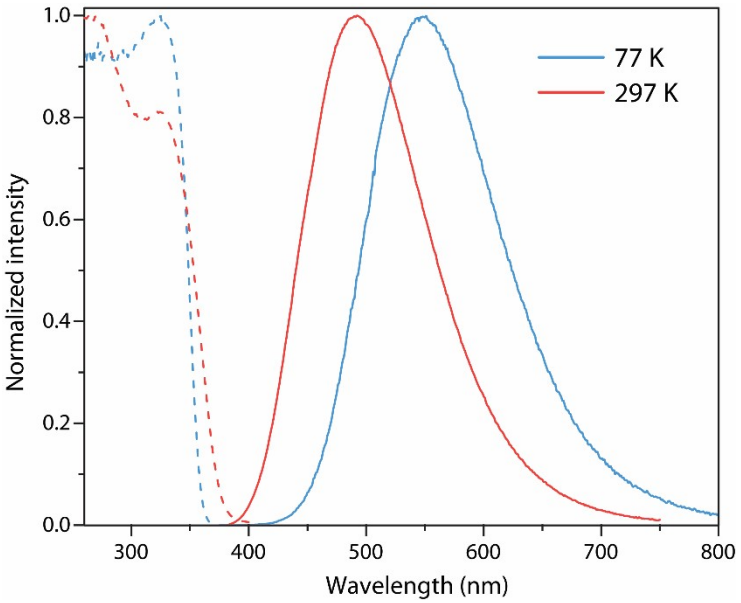

Fig. S16. Normalized excitation (dashed lines) and emission (solid lines) spectra of ***P*^{3}*OO*H** ligand in the solid state.

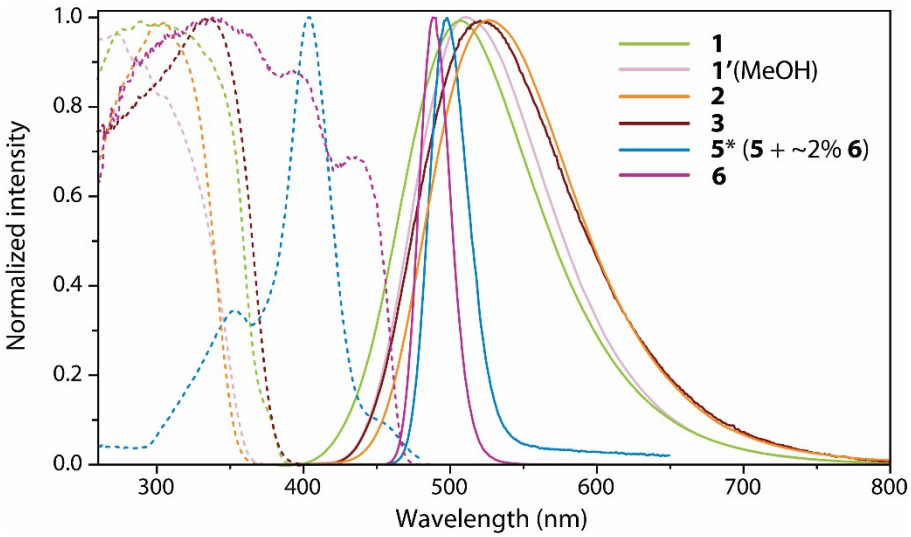

Fig. S17. Normalized excitation (dashed lines) and emission (solid lines) spectra of complexes **1**–**3**, **6** and **5*** (**5** doped with ca. 2% **6**) in the solid state at 77 K.

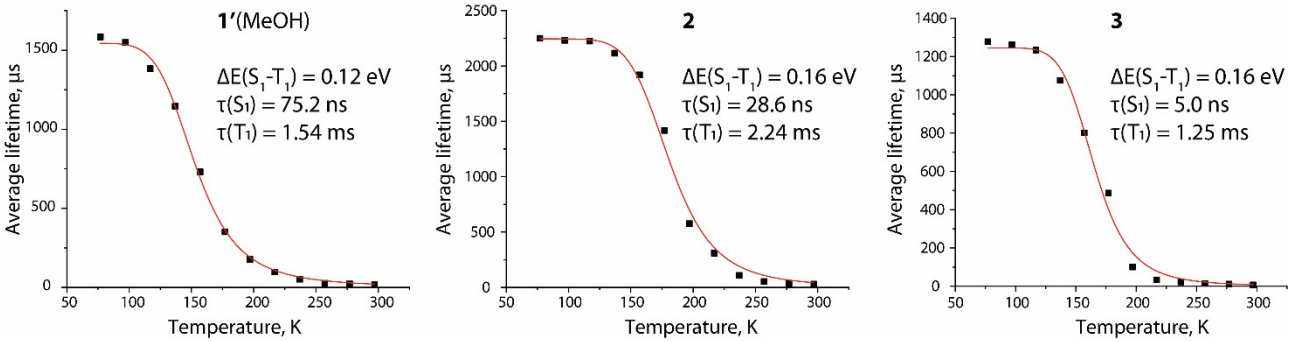

$$\tau_{r\,av}(T) = \frac{3 + \exp\left[-\frac{\Delta E(S_1 - T_1)}{k_B T}\right]}{\frac{3}{\tau(T_1)} + \left[\frac{1}{\tau(S_1)}\right]\exp\left[-\frac{\Delta E(S_1 - T_1)}{k_B T}\right]} \qquad \text{(eqn. S1)}$$

Fig. S18. Temperature dependence of observed average lifetimes of compounds **1**′(MeOH), **2** and **3** in the solid state (excited state characteristics were obtained from the fit based on the two-state model, eqn. S1).

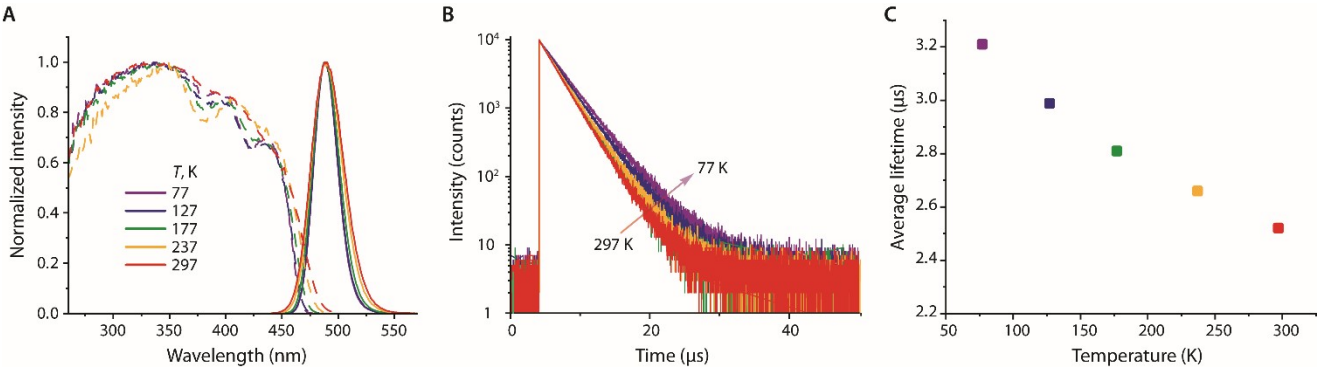

Fig. S19. Variable temperature excitation and emission spectra (A), intensity decays (B), observed average lifetimes of complex **6** in the solid state.

References

1. X. Tan, W. Zeng, X. Zhang, L. W. Chung and X. Zhang, Development of a novel secondary phosphine oxide–ruthenium(II) catalyst and its application for carbonyl reduction, *Chem. Commun.*, 2018, **54**, 535-538.
2. R. Uson, A. Laguna and M. Laguna, (Tetrahydrothiophene)Gold(I) or Gold(III) Complexes, *Inorg. Synth.*, 1989, **26**, 85-91.
3. B. K. Teo, Y. H. Xu, B. Y. Zhong, Y. K. He, H. Y. Chen, W. Qian, Y. J. Deng and Y. H. Zou, A Comparative Study of Third-Order Nonlinear Optical Properties of Silver Phenylacetylide and Related Compounds via Ultrafast Optical Kerr Effect Measurements, *Inorg. Chem.*, 2001, **40**, 6794-6801.
4. M. Beliaeva, A. Belyaev, E. V. Grachova, A. Steffen and I. O. Koshevoy, Ditopic phosphide oxide group: a rigidifying Lewis base to switch luminescence and reactivity of a disilver complex, *J. Am. Chem. Soc.*, 2021, **143**, 15045–15055.
5. I. O. Koshevoy, recent unpublished, recent unpublished.
6. *APEX2 - Software Suite for Crystallographic Programs*, Bruker AXS, Inc., 2010.
7. *CrysAlisPro*, Rigaku Oxford Diffraction, 1.171.43.144a, 2024.
8. G. M. Sheldrick, Crystal structure refinement with SHELXL, *Acta Crystallogr. C: Struct. Chem.*, 2015, **71**, 3-8.
9. L. J. Farrugia, WinGX and ORTEP for Windows: an Update, *J. Appl. Crystallogr.*, 2012, **45**, 849–854.
10. O. V. Dolomanov, L. J. Bourhis, R. J. Gildea, J. A. K. Howard and H. Puschmann, OLEX2: A complete structure solution, refinement and analysis program, *J. Appl. Cryst.*, 2009, **42**, 339-341.
11. G. M. Sheldrick, *SADABS-2008/1 - Bruker AXS Area Detector Scaling and Absorption Correction*, Bruker AXS, 2008.
12. A. L. Spek, PLATON SQUEEZE: a tool for the calculation of the disordered solvent contribution to the calculated structure factors, *Acta Cryst.*, 2015, **C71**, 9–18.
13. M. Nardelli, Modeling hydroxyl and water H atoms, *J. Appl. Cryst.*, 1999, **32**, 563-571.
14. F. Neese, Software update: The ORCA program system - Version 5.0, *WIREs Comput. Mol. Sci.*, 2022, **n/a**, e1606.
15. A. D. Becke, Density-functional exchange-energy approximation with correct asymptotic behavior, *Phys. Rev. A*, 1988, 3098-3100.

16. F. Weigend and R. Ahlrichs, Balanced Basis Sets of Split Valence, Triple Zeta Valence and Quadruple Zeta Valence Quality for H to Rn: Design and Assessment of Accuracy, *Phys. Chem. Chem. Phys.*, 2005, **7**, 3297-3305.
17. F. Weigend, Accurate Coulomb-fitting basis sets for H to Rn, *Phys. Chem. Chem. Phys.*, 2006, **8**, 1057-1065.
18. D. A. Pantazis and F. Neese, All-Electron Scalar Relativistic Basis Sets for the Lanthanides, *J. Chem. Theory Comput.*, 2009, **5**, 2229-2238.
19. D. A. Pantazis, X.-Y. Chen, C. R. Landis and F. Neese, All-Electron Scalar Relativistic Basis Sets for Third-Row Transition Metal Atoms, *J. Chem. Theory Comput.*, 2008, **4**, 908-919.
20. D. A. Pantazis and F. Neese, All-electron scalar relativistic basis sets for the 6p elements, *Theor. Chem. Acc.*, 2012, **131**, 1292.
21. D. A. Pantazis and F. Neese, All-Electron Scalar Relativistic Basis Sets for the Actinides, *J. Chem. Theory Comput.*, 2011, **7**, 677-684.
22. J. D. Rolfes, F. Neese and D. A. Pantazis, All-electron scalar relativistic basis sets for the elements Rb–Xe, *J. Comput. Chem.*, 2020, **41**, 1842-1849.
23. S. Grimme, J. Antony, S. Ehrlich and H. Krieg, A consistent and accurate ab initio parametrization of density functional dispersion correction (DFT-D) for the 94 elements H-Pu *J. Chem. Phys.*, 2010, **132**, 154104.
24. S. Grimme, S. Ehrlich and L. Goerigk, Effect of the damping function in dispersion corrected density functional theory, *J. Comput. Chem.*, 2011, **32**, 1456-1465.
25. J. P. Perdew, K. Burke and M. Ernzerhof, Generalized Gradient Approximation Made Simple, *Phys. Rev. Lett.*, 1996, **77**, 3865-3868.
26. C. Adamo and V. Barone, Toward reliable density functional methods without adjustable parameters: The PBE0 model, *J. Chem. Phys.*, 1999, **110**, 6158-6170.
27. E. F. Pettersen, T. D. Goddard, C. C. Huang, G. S. Couch, D. M. Greenblatt, E. C. Meng and T. E. Ferrin, UCSF Chimera—A visualization system for exploratory research and analysis, *J. Comput. Chem.*, 2004, **25**, 1605-1612.